Development of pollinated and unpollinated ovules in *Ginkgo biloba*: unravelling pollen's role in ovule tissue maturation

Antonella Muto[a], Emanuela Talarico[a], Greta D'Apice[b,c], Maurizio Di Marzo[d], Silvia Moschin[b,c], Sebastiano Nigris[b,c], Nicola Babolin[d], Eleonora Greco[a], Fabrizio Araniti[e], Adriana Chiappetta[a], Lucia Colombo[d] , Barbara Baldan[b,c], Leonardo Bruno[a†]

[a] *Department of Biology, Ecology and Earth Sciences (DiBEST), University of Calabria, 87036 Arcavacata of Rende (CS), Italy*

[b] *Botanical Garden, University of Padova, 25123 Padova, Italy*

[c] *Department of Biology, University of Padova, 35121 Padova, Italy*

[d] *Department of Biosciences, University of Milano, 20133 Milano, Italy*

[e] *Department of Agricultural and Environmental Sciences - Production, Landscape, Agroenergy, University of Milano, 20133 Milano, Italy*

†Corresponding author

Email addresses: Antonella Muto antonella.muto@unical.it
Emanuela Talarico emanuela.talarico@unical.it
Greta D'Apice greta.dapice@studenti.unipd.it
Maurizio Di Marzo maurizio.dimarzo@unimi.it
Silvia Moschin silvia.moschin@unipd.it
Sebastiano Nigris sebastiano.nigris@unipd.it
Nicola Babolin nicola.babolin@unimi.it
Eleonora Greco eleonora.greco@unical.it
Fabrizio Araniti fabrizio.araniti@unimi.it
Adriana Chiappetta adriana.chiappetta@unical.it
Lucia Colombo lucia.colombo@unimi.it
Barbara Baldan barbara.baldan@unipd.it
Leonardo Bruno leonardo.bruno@unical.it

ABSTRACT

In gymnosperms such as *Ginkgo biloba*, the pollen's arrival plays a key role in ovule development, before fertilization occurs. Accordingly, *G. biloba* female plants geographically isolated from male plants aborted all their ovules after the pollination drop emission, which is the event that allows the ovule to capture pollen grains. To decipher the mechanism induced by pollination required to avoid ovule senescence and then abortion, we compared the transcriptomic of pollinated and unpollinated ovules at three time points after the end of the emission of pollination drops. Transcriptomic and *in situ* expression analyses revealed that several key genes involved in programmed cell death such as senescence and apoptosis, DNA replication, and cell cycle were differentially expressed in unpollinated ovules compared to pollinated ones. Interestingly, we provided evidence that the pollen captured by the pollination drop affects auxin local accumulation and might cause the deregulation of key genes required for ovule's programmed cell death and activating both the cell cycle and DNA replication genes.

KEYWORDS

Auxin, Female Gametophyte, Gymnosperm, Ovule, Pollen, Senescence, Transcriptome, Transcription factors.

ABBREVIATIONS

DAD, Days After Drop; DEG, Differentially Expressed Gene; FCL, Flattened-Cells Layer, FG, Female Gametophyte; FM, Functional Megaspore; FNMM, Free Nuclear Mitosis of the Megagametophyte; GO, Gene Ontology; ISH, *In Situ* Hybridization, KEGG, Kyoto Encyclopaedia of Genes and Genomes; MMC, Megaspore Mother Cell; PCD, Programmed Cell Death; PCW, Pollination condition by WGCNA; PD, Pollination Drop; PO, Pollinated Ovules; TF, Transcription factor; UO, Unpollinated Ovules; WGCNA, Weighted Gene Correlation Network Analysis.

INTRODUCTION

Ovule development is a complex process conserved in angiosperms and gymnosperms, from the sporangium formation to the Functional Megaspore (FM) differentiation (Yadegari and Drews, 2004). The ovule structure is constituted by a megasporangium (nucellus) protected by one or more sterile outer integuments. Integuments are initiated as annular outgrowths and ultimately extend upwards around the nucellus to delimit the micropyle. This apical opening allows the male gametophyte to deliver one or more male gametes inside the Female Gametophyte (FG) (Rudall, 2021). The FG is formed by a multistep process consisting of two phases: megasporogenesis and megagametogenesis (Yadegari and Drews, 2004). The megasporogenesis initiates with the differentiation of a single cell near the nucellus named Megaspore Mother Cell (MMC), which, through a meiotic division, will originate a tetrad of spores. Only the most basal spore of the tetrad persists and originates the FG through Free Nuclear Mitosis of Megagametophyte (FNMM) (Douglas *et al.*, 2007). Then, in several gymnosperms, cellularization generates a FG that differentiates two archegonia, each bearing one egg cell (Zhang and Zheng, 2016). Overall, ovules are formed by sporophytic tissues such as the integument(s) and the FG, each performing a specific function controlled by complex genetic and molecular networks controlling cell proliferation, specific cell commitment and differentiation, as well as Programmed Cell Death (PCD) during different developmental stages.

So far, the genetic networks and molecular mechanisms controlling ovule development have been extensively investigated in angiosperms, using model species such as *Arabidopsis thaliana* (Drews and Koltunow, 2011; Cucinotta *et al.*, 2014, 2020). Although relevant contributions have been added recently, ovule development in gymnosperms is still largely unexplored (Shigyo *et al.*, 2006; Yamada *et al.*, 2008; Chen *et al.*, 2017; Zumajo-Cardona *et al.*, 2021). Recent works have investigated in particular the genetic and molecular pathways during ovule development in *Ginkgo biloba* through an integrated approach encompassing morphological, transcriptomic, metabolomic (D'Apice *et al.*, 2021) and *In Situ* Hybridization (ISH) analyses (Zumajo-Cardona *et al.*, 2021; D'Apice *et al.*, 2022).

In *Arabidopsis*, as in several angiosperms, double fertilization, which is temporally close to the pollination event, is required for further differentiation of ovule integuments into seed coats (Figueiredo *et al.*, 2016; Figueiredo and Köhler, 2018). Differently, in *Ginkgo*, where pollination is separated by fertilization through a long time (i.e. four/five months), the signal for further ovule development and FG differentiation is provided by the arrival of pollen in the pollination chamber, which triggers the differentiation of three distinguishable layers in the ovule integument, driving its transformation into the seed coats long before fertilization takes place (D'Apice *et al.*, 2021, 2022).

In line with these observations, *Ginkgo* female plants geographically isolated from male plants aborted all their ovules after the Pollination Drop (PD) emission, which in this species allows the identification of the ovule receptive phase to pollination (Friedman, 1987). In *Arabidopsis*, it has been demonstrated that PCD process occurs in the tissue of the unpollinated stigmas. In particular, transcriptional profiling revealed that NAC Transcription Factors (TFs) *ORESARA1* (*ORE1*) and *KIRA1* (*KIR1*) activated the senescence program in unpollinated pistils (Gao *et al.*, 2018).

In this work, we aimed to study the pollen-induced molecular pathway in *Ginkgo biloba*, which promotes the ovule development into a seed, repressing a senescence program.

To this aim, we performed a transcriptomic analysis on ovules collected immediately after the pollination time from both female plants that received pollen and from plants geographically isolated and unable to receive pollen.

The pollination time was easily identified due to *Ginkgo*'s characteristic, common to many gymnosperms, of secreting a drop from the ovule sporophytic tissue through the micropylar canal. This drop captures the pollen and drags it inside the ovule, where it will germinate (Prior *et al.*, 2019).

The expression analysis we performed on selected genes sheds light on some molecular mechanisms that regulate FG development in this gymnosperm. Our data also supported the hypothesis that local auxin accumulation plays a fundamental role in ovule development, affecting both nucellus degeneration and FG development, even in gymnosperms. Interestingly, we have identified several key pathways related to ovule development, such as hormone signalling, senescence and apoptosis, cell cycle, DNA replication and damage repair, as well as the down-regulation of ATP synthesis-related proteins that are differentially regulated in Pollinated and Unpollinated Ovules (PO and UO respectively). Our results suggest that the pollen triggers the initiation of ovule enlargement and further differentiation inhibiting PCD, particularly key genes related to the senescence and apoptosis pathway and activating switches genes related to hormone signalling, DNA replication and cell cycle regulation.

MATERIAL AND METHODS

Plant material

Pools of PO and UO were collected during the pollination timeframe (March and April 2021). PO were collected from ten female plants at the Botanical Garden of the University of Calabria, Cosenza, Italy (39° 17′ 43″ N, 16° 15′ 13″ E) while UO were collected from 10 female and isolated plants located in the Coretto Garden (CS) Calabria (39°41’49’’ N, 16°25’43’’ E). Ovules were

collected at stages 6, 7 (stages before the pollination event), stage 8.1 (drop emission stage) and three stages after the end of the drop emission (Days After Drop, DAD), respectively 1 (UO_1, PO_1), 6 (UO_6, PO_6), and 8 days (UO_8, PO_8), as described in D'Apice *et al.* (2021).
For the molecular analyses, thirty ovules for each stage were pooled from 10 plants during the growing season for both conditions. Samples were immediately frozen into liquid nitrogen and stored at -80°C.

Morphometric analyses

A total of thirty PO and UO from each stage analysed, respectively UO_1, UO_6, UO_8, PO_1, PO_6, and PO_8 were randomly collected from different trees and used for size measurement. Ovules were measured considering the diameter at the broadest part, using the software ImageJ (Schneider *et al.*, 2012). Statistical analyses were performed on diameter values, first testing the homogeneity (Leven Median test) and then analysed by ANOVA and Tukey's rank test ($P < 0.05$).

Paraffin embedding and sample section observations

For each stage analysed, at least twenty-five ovules randomly collected from different trees were processed, as reported by D'Apice *et al.* (2021). Ovules were fixed in 4% (w/v) paraformaldehyde in Phosphate Buffer Saline (PBS) (10XPBS: 1.3M NaCl, 70 mM Na_2HPO_4, 30mM NaH_2PO_4; pH 7.4) with vacuum infiltration and then left overnight in fixative at 4°C. The next day, samples were dehydrated by using ethanol series (30%, 50%, 70%, 85%, 95% in distilled sterile water for 1 h each step) and subsequently ethanol was replaced using a xylene series (25%, 50%, 75% and 100% for 1 h each step). Lastly, xylene was gradually replaced by Paraplast Plus (Fisher Scientific), with changes every day. Ovules embedded were maintained at 4°C until they were processed, and sections of 10 µm were cut with Leica RM2125RT microtome. Slides were deparaffinised and rehydrated to be stained with 0.05% (w/v) toluidine blue. Histological sections were analysed by Leica DRMB microscope to determine their developmental stage, and images were acquired with the digital camera Leica DFC 320 (Leica, Milan, Italy).

RNA isolation and RNA sequencing library synthesis

Total RNA extraction was performed separately for each of the 18 samples (three biological replicates of a pool of ovules were used for each of the three stages analysed for PO and UO) using 100 mg of the ovule powder according to the manufacturer's recommendations of Agilent Total

RNA Isolation Mini Kit (Agilent Technologies, Santa Clara, CA, USA). cDNAs were then processed for libraries preparations by NOVOGENE Services and sequencing with Illumina HiSeq 2500 RNA-Seq. (50M,15G) platform (Illumina, San Diego, CA) to generate pair-end reads of 150 bp for each fragment. Statistics of RNA-Seq alignment for all the 18 libraries obtained was reported in **Supplementary Table S1**. Raw data are deposited with the code Bioproject PRJNA700482 as Sequence Read Archive (SRA) data. Strand-specific libraries were constructed from mRNA of both UO and PO collected 1, 6, and 8DAD. DESeq2 was then used to identify significant pollination-associated gene expression changes in ovule samples. Differentially Expressed Genes (DEGs), with a p-adjusted <0.05 and |log2 (ratio)| > 1.5, as the thresholds to determine the significance of DEGs, were identified after pairwise comparisons between libraries of the same time points (UO_1/PO_1; UO_6/PO_6; UO_8/PO_8).

Weighted gene co-expression network analysis (WGCNA)

Co-expressed DEGs were identified by a scale-free WGCNA (Pearson's correlation coefficient ≥ 0.65 and $p \leq 0.05$), and a soft threshold value, power of 16, was used to transform the adjacency matrix to meet the scale-free topology criteria for optimal clustering (Langfelder and Horvath, 2008). Module-trait relationship figures were created in the R environment. A matrix of 14914 relatively highly expressed genes (FPKM > 10 in any sample) was filtered and applied to WGCNA. Modules were designated by a colour and consisted of genes with similar expression patterns when referring to the "Pollination condition" trait. Genes belonging to the same module showed highly correlative expression patterns (Hollender *et al.*, 2014). "Pollination condition" trait data were used for correlation network analyses with gene expression trends.

Real-Time Quantitative PCR (RT-qPCR) analysis

To validate the expression of selected genes, identified based on Illumina RNA-Seq results, quantitative real-time PCR experiments were performed according to D'Apice *et al.* (2021). Primer sequences were reported in **Supplementary Table S2**. As RNA-Seq (FPKM) and RT-qPCR produce relative gene expression measures, Pearson correlation coefficient calculation was used for each pair of genes selected, to evaluate concordance in gene expression.

In situ hybridization

Chemical fixation and tissue processing for the RNA *in situ* hybridization were performed as described by D'Apice *et al.* (2022) and above, considering at least thirty PO and UO from each stage analysed. The sequences of the probes are listed in **Supplementary Table S2**. Target sequences were amplified with primers containing the T7 sequence at the 5' of forward primer (sense) and the 5' of reverse primer (antisense) sites from cDNA obtained from total RNA retrotranscribed using the Invitrogen SuperScript III kit (Invitrogen, Waltham, Massachusetts, USA). The PCR products were then used for in vitro transcription using DIG-11-UTP, as described in the DIG RNA labelling kit (Roche Diagnostics GmbH, Mannheim, Germany) and stored at −20 °C before hybridization. Tissue treatments, pre-hybridization, post-hybridization washes and antibody treatment were performed according to the protocol described by Ambrose *et al.* (2000). Probes were hybridised overnight at 55°C in 50% formamide humidified box. The anti-DIG-AP Fab fragments antibody (Roche Diagnostics GmbH, Mannheim, Germany) was diluted 1:700 and incubated for 2 h at room temperature. Detection was then developed overnight using the NBT/BCIP detection solution (Roche Diagnostics GmbH, Mannheim, Germany). Slides were then washed in stop buffer (100 mM Tris-HCl, pH 8.0; 1 mM EDTA), dehydrated, and mounted with Canada balsam (CARLO ERBA Reagents). Images were captured using a Leica DFC 320 digital camera (Leica, Milan, Italy).

Immunohistochemical localization of indole-3-acetic acid (IAA)

A total of thirty PO and UO from each stage analysed were randomly collected from different trees after the end of emission of the pollination drop. Immunolocalization was performed as described in Chiappetta *et al.* (2009). Ovules were collected and fixed in a 3% (w/v) paraformaldehyde and 0.5% (v/v) glutaraldehyde mixture in 1X PBS buffer (10XPBS: 135 mM NaCl, 2.7 mM KCl, 1.5 mM KH_2PO_4, 8mM K_2HPO_4, pH 7.3). Longitudinal sections of thick of 50 µm were cut by a vibratome (Leica VT1000E, Germany) and incubated with anti-IAA monoclonal primary antibody (Sigma-Aldrich) diluted 1:250 in PBS/BSA solution (10 mM phosphate solution, 0.8% bovine serum albumin) overnight at 4 °C. The next day, sections were washed (3x10 min) and incubated with the secondary antibody (anti-mouse IgG alkaline phosphatase conjugate; Promega Italia, Milan, Italy) diluted 1:150 in 1X PBS solution for 3 h at room temperature. Detection was performed with NBT (4-Nitro blue tetrazolium chloride) and BCIP (5-bromo-4-chloro-3-indolylphosphate) mix, then rinsed with blocking buffer (100 mM Tris-HCl, pH 8.0; 1 mM EDTA). Control samples were processed without primary IAA antibody. Images were taken with a Leica DRMB microscope equipped with a Leica DFC 320 camera (Leica, Milan, Italy).

In situ detection of DNA fragmentation (TUNEL assay)

Ginkgo ovules (fifteen) for each analysed stage, respectively UO_1-8, PO_1-8, were fixed in 4% (w/v) paraformaldehyde in 1X PBS overnight at 4 °C. Next day, the samples were dehydrated through ethanol series, as described above, and embedded in Paraplast Plus (Sigma-Aldrich).

Sections of 10 µm were cut and stretched on poly-L-lysine coated slides. Sections were then dewaxed in the xylene series and re-hydrated. According to the manufacturer's instructions, TUNEL assay was performed using "Click-iTTM Plus TUNEL Assay" (Thermo Fisher Scientific).

The labelling reaction was performed in the dark for 1 h in a humidified chamber at 37 °C. A negative control was obtained by excluding TdT from the reaction mixture. As a positive control, some sections were incubated with DNase I ($1Uml^{-1}$) for 30 minutes at room temperature before the TUNEL assay.

Confocal images of median longitudinal sections were obtained using a Leica inverted TCS SP8 confocal scanning laser microscope. The detection of green fluorescence of incorporated EdUTP-Alexa FluorTM 488 (excitation peak centred at 495 nm, emission peak wavelength of 519 nm), and DAPI staining ($1\ gml^{-1}$) (excitation peak centred at 358 nm, emission peak wavelength of 461 nm) were performed by combining the settings indicated in the sequential scanning microscope facility.

RESULTS

Lack of pollination event induces dramatic changes in ovule size and morphology

To unravel the role of pollination on ovule development, we elaborated the growth kinetics by measuring the diameter of PO and UO starting from the opening of buds (Stage 6) to 10 days after the end of PD emission. Although the emission of PD occurred in middle April in both sites (see Material and Methods), the isolated female plants had a significant extension of this stage. It lasted approximately one week in plants in which pollination occurred and about two weeks in isolated unpollinated female plants (**Fig. 1A**). No significant difference in ovule size in both sites until the PD emission (stage 8.1) were observed. After PD emission, the size of PO grew rapidly. At the same time, UO decreased in size and initiated a senescence process leading to ovules dropping in the middle of May (**Fig. 1A**). Based on these evidences, we performed histological analysis on ovules collected at the following stages: PO_1, PO_6, PO_8, UO_1, UO_6, UO_8. At the PO_1 and UO_1, observing differences at the cyto-histological level. In particular, at the UO_1, a slight loss of tissue integrity and organisation was observed in the most basal regions of the nucellus, similar to a laceration initiation (**Fig. 1E**). However, the integument was formed, the micropyle presented

the characteristic teardrop shape, and the FG was in a coenocytic stage (**Fig. 1B, E**). In PO_6, the cells surrounding the pollen chamber collapsed inward, reducing its narrow opening. In this stage, the FG presented multiple nuclei enclosed in a single cell, typically resulting from nuclear divisions uncoupled from cytokinesis (**Fig. 1C**). Indeed, at the centre of FG was located a large vacuole surrounded by several dozen free nuclei. Until the last stage, free nuclei filled towards the centre and their number in PO dramatically increased. In contrast, in UO_6 the FG were empty of free nuclei, resulting in a bigger vacuole size. Moreover, in UO_6, a tissue laceration was observed in the Flattened-Cells Layer (FCL) in all ovules analysed (**Fig. 1F**). At the last stage, in PO_8, FG was growing, the tapetum was degenerating, and the three layers of the integument were completely distinguishable (**Fig. 1D**). Instead, in UO_8 stage, the morphology of the ovule was completely altered, the nucellus appeared disorganised and the tissue laceration in the FCL was more extended when compared to UO_6 (**Fig. 1G**). Based on our observations, we concluded that pollination prevents the ovule cyto-histological disorganisation and allows ovule development progression.

Pollination causes dramatic changes in ovule transcriptome

To investigate the genetic and molecular networks controlling ovule response to pollination in *Ginkgo*, we performed a transcriptomic analysis on ovules collected from both plants that received pollen and unpollinated plants. A total of 6394 DEGs linked to pollination were identified from these pairwise comparisons (**Fig. 2A**). In particular, the UO_1/PO_1 list contained 1274 DEGs (651 upregulated and 623 downregulated), UO_6/PO_6 had 4471 DEGs (2383 upregulated and 2088 downregulated) and UO_8/PO_8 had 3400 DEGs (1177 upregulated and 2223 downregulated) (**Fig. 2A**). In addition, we further investigated conserved and stage-specific DEGs between subsequent developmental stages using a Venn diagram (**Fig. 2B**). As expected, the highest number of stage-specific DEGs (2139, 33.5% of total) were found in the comparison of UO_6/PO_6, followed by UO_8/PO_8 (with 1276, 20% of total), while the lowest number of stage-specific DEGs (530, 8.3% of total) was found in the comparison at 1DAD. These data suggested that several biological processes dramatically changed from 1DAD to 6DAD in the ovules after the pollination event. We also identified 300 (4.7% of total) conserved DEGs in all three comparisons analysed (**Fig. 2B**). Gene Ontology (GO) enrichment analysis, performed for DEGs in each of the comparisons for both UO and PO, showed that most of the DEGs were enriched in response regulation pathways, such as several abiotic and biotic stress response categories as defence response to fungi or defence response to bacteria and wounding (**Supplementary Fig. S1A-C**). Also GO terms involved in stimuli and hormones, particularly ethylene and auxin-activated signalling pathways, regulation of transcription DNA-templated, methylation, and lipid catabolic process were also significantly

impacted (**Supplementary Fig. S1A-C).** Kyoto Encyclopaedia of Genes and Genomes (KEGG) enrichment analysis showed that the most impacted pathways were those for phenylpropanoid biosynthesis, flavonoid biosynthesis, mismatch repair, DNA replication, homologous recombination, cutin, suberin and wax biosynthesis, and plant hormone signal transduction (**Supplementary Fig. S2A-C**).

Pollination-specific modules were then identified using WGCNA. The WGCNA, considering the 14914 genes with FPKM > 10, resulted in sixty distinct modules (**Supplementary Table S3, Fig. S3A, B**). Indeed, 7906 genes (**Supplementary Table S3**), grouped in nineteen modules, were found to be correlated significantly and specifically with the "Pollination condition" trait (**Supplementary Fig. S3A, B; Supplementary Table S3, S4**). We overlapped the DEGs UO/PO list and the "Pollination condition by WGCNA" (PCW). The frequency of the module with the DEGs UO/PO listing was shown in **Supplementary Fig. S4**. The combination of these two approaches, identified genes of interest involved in specific pathways such as hormone metabolism, PCD (senescence and apoptosis), cell cycle regulation and mitosis, DNA replication and damage repair (**Fig. 2C**), strongly impacted by pollination signal (**Supplementary Table S5, S6, S7)**. All the RT-qPCR results support the reliability of the RNA-Seq analysis (**Supplementary Fig. S5**).

Auxin homeostasis is differentially regulated depending on the pollination event

Most DEGs were related to hormones biosynthesis and signalling (**Supplementary Fig. S6**), so we decided to focus on auxin because it is well characterised its role in ovule development in other species (Barro-Trastoy *et al.*, 2020; Cucinotta *et al.*, 2021). Concerning the auxin pathway, 27 genes were included in both DEGs and PCW lists (**Supplementary Table S5**). A heat map with this fraction involved in the auxin pathway was created to summarise the gene expressions in both conditions in the three time points analysed (**Supplementary Fig. S7**). PO showed a higher expression of auxin-related genes, especially in UO_6/PO_6 comparison. Notably, auxin efflux carriers (PINs) play a key role in ovule auxin accumulation. In this work, we investigated the *Ginkgo* orthologous of *AtPIN1* (*Gb_06199*) by ISH, given the known importance in ovule initiation and development (Ceccato *et al.*, 2013). In PO_1, *Gb_06199* mRNA signal was widespread, but more intense in the flap (**Fig. 3A**), whereas in PO_6 it was localised in the nucellus, integument and flap zone (**Fig. 3B**). Instead, in PO_8 the signal was restricted to the FG and flap zone (**Fig. 3C**). Regarding UO, in the first stage, *Gb_06199* transcripts were detected in the flap and in the nucellus (**Fig. 3E**), whereas in UO_6 and UO_8 they appeared widespread and not specifically localised, except for a cluster of marked cells around the FG (**Fig. 3F, G**).

In this context, the endogenous levels of free IAA were also estimated in PO and UO (**Fig. 4**). In PO_1, the IAA signal was intense and distributed throughout all ovule tissues (**Fig. 4A**). In PO_6, the signal was more restricted to the chalaza zone (**Fig. 4D**), the pollen chamber, and the integuments at the micropylar level (**Fig. 4B**). In PO_8 ovules the signal was weak and spread over the ovule tissues (**Fig. 4G**). Interestingly, clusters of marked cells around the gametophyte of PO in all the stages were observed (**Fig. 4D-E, H**). Regarding UO, in both UO_6 and UO_8, auxin accumulation is quite comparable. Indeed, the integuments and tapetum were strongly stained, but no clusters of marked cells around the gametophyte were evident (**Fig. 4C, F, I**).
The findings indicate an organized auxin distribution pattern within the nucellus of PO. Conversely, in the absence of pollination, this distribution appears disorganized in the ovule.

***NAC* and *MYB* genes are differentially expressed upon pollination**

Among the DEGs between PO and UO, 96 TFs, represented by 37 different families, were in common between DEGs and PCW lists (**Supplementary Table S8**). Heat maps were created to illustrate the variations of 96 TFs gene expression in the stages analysed (**Supplementary Fig. S8**). Considering the involvement of *MYB* and *NAC* genes in ovule development (Schubert *et al.*, 2019; Zhang *et al.*, 2021), we analysed the expression domains of selected MYB and NAC encoding genes. ISH was performed comparing stages UO_6 and PO_6, as this comparison showed the most significant differences in gene expression changes based on RNA-Seq results. *MYB Gb_15607* was localised in the degenerated FG of UO (**Fig. 5B**). A weaker expression of the gene was also visible in the FG of PO at the same stage (**Fig**. **5A**). *R2R3MYB5* (*Gb_02997*) was only and weakly expressed in the tapetum of the PO (**Fig. 5C**), while no expression was localised in UO (**Fig. 5D**). *R2R3MYB25* (*Gb_39852*) was expressed in the degenerating nucellus and the innermost part of the UO integument (**Fig. 5F**), while in the PO the localization was slightly visible in the tapetum (**Fig. 5E**). *NAC Gb_05670* was expressed in the degenerating nucellus of UO and in the flanking integument (**Fig. 5J**). Instead, the signal of *Gb_05670* in PO was slightly visible in the FG (**Fig. 5I**). In addition, *NAC Gb_13930* was strongly expressed in the FG of the UO (**Fig. 5L**), while it was weakly visible in the FG of the PO (**Fig. 5K**). Interestingly, *NAC Gb_35309* and *Gb_18916* showed patterns of expression similar to *Gb_05670*. Indeed, they are expressed in the degenerated nucellus and in the integument of UO (**Fig. 5N, P**). In PO, their expression was weak but widespread through the nucellus and in the inner part of the integument (**Fig. 5M, O**). Longitudinal sections of PO and UO hybridised with sense probe for each gene are reported in **Supplementary Fig. S9**.

Genes related to PCD, cell cycle regulation, DNA replication and damage repair exhibit a different expression in pollinate respect to unpollinated ovules

Through bioinformatic analysis we selected 27 senescence-related genes (**Supplementary Table S6**), 9 of which were in common between DEGs and PCW lists: 1 Cysteine proteinase (*CYSP*), 3 Metacaspase (*MCA*), 1 KDEL-tailed cysteine endopeptidase (*CEP1*), 2 Ribonuclease 1 (*RNS1*), 2 Autophagy-related protein (*ATG*). Considering apoptosis metabolism, among 36 genes found (**Supplementary Table S6**), only a Proteasome Subunit Beta (*PSB3*, *Gb_09326*) gene was in common between the two lists.

The common genes analysed (10) displayed higher expression levels in the UO_6 and UO_8 compared to PO stages, except for the *PSB3 Gb_09326*, which exhibited an opposite trend (**Supplementary Fig. S10**). In plants, most of the enzymes acting in PCD belong to cysteine protease (CYSP) family (van Doorn and Woltering, 2008). Consequently, we analysed *CYSP1 Gb_13610* expression pattern in ovules by ISH. In PO_1 and PO_6, *CYSP1* expression was localised in all tissues of the ovules with a higher signal in the nucellus as well as in the flap zone (**Fig. 6A-B**). In PO_8, *CYSP1* expression was confined in the nucellus and around the FG (**Fig. 6C**). Concerning UO_1, no differences were observed when compared to the PO_1 (**Fig. 6A, E**). In both UO_6 and UO_8, *CYSP1* was expressed in all ovule tissues, with a strong localization around the FG (**Fig. 6F-G**).

The histological analysis showed an abnormal FG development in UO samples, suggesting defects in karyokinesis that might indicate cell cycle misregulation. RNA-Seq data analysis supported this observation. Indeed, considering both DEGs and the PCW lists, we selected 9 key common genes encoding regulators of the cell cycle and mitosis (**Supplementary Table S7**), whose expression is shown in the heat map (**Supplementary Fig. S11**). Among these 9 genes, we analysed *Cyclin-dependent kinase B1-1* (*CDKB1*) *Gb_38629* localization (**Fig. 7**), given the known role in the regulation of cell cycle progression (Umeda *et al.*, 1999; Porceddu *et al.*, 2001). *CDKB1* (*Gb_38629*) was downregulated in UO with respect to pollinated ones and its expression was detected in all PO stages in the FG, nucellus and FCL (**Fig. 7A-C**). The same localization was found in the UO at the same stages, with a gradual decrease in the signal (**Fig. 7E-G**).

Considering genes related to DNA replication and damage repair, 28 were in common among the two lists (**Supplementary Table S7**). The expression trend of the 28 genes was illustrated in **Supplementary Fig. S12**. All the genes showed a higher expression in the PO compared to UO in all developmental stages analysed, although the most significant difference was found at 6DAD (**Supplementary Fig. S12**).

PCD detection of aborted ovules

To determine how early cell degeneration starts in UO as cytological features and transcriptomic dataset suggest, TUNEL assay was applied in longitudinal sections of UO and PO (**Fig. 8; Supplementary Fig. S13**). Specifically, at UO_1, DNA fragmentation was observed exclusively in the basal zone of the nucellus, where, according to cyto-histological analysis, tissue degeneration and cavity will be evident in later stages (**Fig. 8D**). In the last stages, UO_6 (**Fig. 8E**) and UO_8 (**Fig. 8F**), several nuclei were TUNEL positive differently from PO, where a sporadic signal is localised in the integument (**Fig. 8A-C)**. This experiment confirms our hypothesis that in UO, a PCD program immediately starts in the absence of pollination, and we concluded that pollination inhibits the PCD program in PO.

DISCUSSIONS

Microstructure of pollinated and abortive ovules

Based on morphological observations, we have hypothesised that pollination could be the signal for further ovule development and FG differentiation, leading to the formation of three distinguishable layers in the ovule integument, driving its transformation into the seed coats long before fertilization takes place (D'Apice *et al.*, 2021, 2022). In gymnosperms, molecular evidences suggesting that the pollination process stimulates the gene expression changes required for ovule developmental progression have not been described. This is due to the difficulty to investigate pollen signalling in the field, and to the scarcity of ovule mutants in these species. (Lu *et al.*, 2016). In addition, in *Ginkgo*, which possess orthotropes ovules, pollination drops capture pollen from the environment, and transport it inside the nucellus (Jin *et al.* 2012). During this process, pollen grains are hydrated on the surface of the PD and enter into the nucellus acquiring the chance of fertilising the egg cell (Jin *et al.*, 2012). It has been demonstrated that viable pollen sank faster than unviable pollen, suggesting an effective screening mechanism for *Ginkgo* (Jin *et al.*, 2012; Lu *et al.*, 2016).

Pollen arrival is crucial for ovule development progression. Actually, *Ginkgo* female plants isolated from male plants aborted all their ovules after the pollination drop (Friedman, 1987). Starting from this observation, this study aimed to explore the possible mechanism associated with ovule abortion in unpollinated *Ginkgo* ovules by combining anatomical observations and a transcriptomic approach. The relation between ovule development and a successful pollination suggests a strict communication between the ovule integument, the FG, and the male gametophyte. Indeed, in our studies, the PD in *Ginkgo* pollinated plants lasted for approximately 7 days, while unpollinated plants showed a prolonged period of PD production. According to Jin *et al.* (2012), these results suggested that plants invest energy to persistently secrete abundant PDs during the

pollination period, contrasting the evaporation effect of wind and sunlight. In addition, the inner structures of the pollinated and abortive ovules were considerably different. Indeed, the presence of a cavity in the basal portion of the nucellus in UO is in line with results obtained in other species, such as *Punica granatum* (Wetzstein *et al.*, 2013), *Cucumis sativus* (Li *et al.*, 2014) and *Camellia oleifera* (Gao *et al.*, 2017). Moreover, in *Prunus mume* Sieb. et Zucc. the absence of reproductive events induces anomalies in embryo sac development and differentiation (Sun *et al.*, 2016).

Differential expression of some ovule-related genes might affect the growth of *G. biloba* ovule

RNA-Seq approach was used to investigate the genetic pathways involved in ovule abortion in the absence of pollination event. Thus, the differences in gene expression between UO and PO at three developmental stages were analysed. The data revealed that most of the DEGs were found at 6DAD, suggesting that the responses to the pollination occurred about one week after pollen arrival. Interestingly, this stage coincides with the germination of the male gametophyte (Friedman, 1987). It is therefore possible to assume that this process also plays a crucial role in determining the large number of DEGs at 6DAD. Accordingly, Yao and collaborators (2018) revealed extensive changes in the transcriptome of the gymnosperm *Pinus tabuliformis* during the FNMM between the Fertile Line (FL) and Sterile Line (SL). In this study, 7174 DEGs were found at three developmental stages, named FNM1, 2 and 3. The highest number of DEGs was found at FNM2, suggesting the evident differences in the transcriptional level at FNM2.

Our functional GO annotation has revealed that the most of the significant DEGs fell into the biological processes categories of hormones, senescence, cell cycle, stress and defence response genes. In accordance, Gong *et al.* (2021) performed a similar study, investigating the transcriptomic data of natural ovule abortion mutants (female sterile line, STE) and the wild type (female fertile line, FER) of *Pinus tabuliformis* Carr. Upon comparing our GO analysis with that conducted by Gong and colleagues, we found a nearly complete overlap of the GO terms. This indicates that in gymnosperms, the lack of pollination leads to abnormal mitosis and apoptosis.

Both auxin signalling and Programmed Cell Death are essential for ovule developmental progression in *G. biloba*

Auxin has been studied due to its significant role in ovule development (Larsson *et al.*, 2017), in addition to being one of the strongly impacted pathways.

In different species, pollination and subsequent fertilization induced the rapid accumulation of several hormones, including auxin and gibberellins, which play key roles in the induction of the fruit set (Dorcey *et al.*, 2009; McAtee *et al.*, 2013). Moreover, recent studies indicate that cellular

preparation for PCD is coordinated primarily by transcriptional regulation of hormone signalling (Li *et al.*, 2022; Ni *et al.*, 2022; Guo *et al.*, 2023). In particular, auxin signalling and PCD regulation seem to be often connected (Kacprzyk *et al.*, 2022).

Thus, in this work, we mainly focused on the crosstalk between auxin and PCD during *Ginkgo* ovule development, focusing on its impact on degeneration of the nucellus. In the ovule, the nucellus is a short-lived tissue that, as it degenerates, allows the expansion of the FG (Domínguez *et al.*, 2001), in both gymnosperms and angiosperms (Daneva *et al.*, 2016).

Although a set of DEGs involved in hormone signalling and nucellar cell death were identified (Li *et al.*, 2019), the molecular network controlling the nucellar PCD in *Ginkgo* ovules has not been well understood.

In a previous work (D'Apice *et al.*, 2021), we showed that during stage 9, the micropyle opening is narrower, and nucellus cells adjacent to the pollen chamber collapse inward, gradually reducing its dimension until closing it. Then, the haustorial pollen tube consumes the nucellar tissue, which is also thinning because of the expansion of the coenocytic FG. This generally forms more than one thousand free nuclei before cellularization begins (Lee, 1955).

In *Arabidopsis*, a part of the nucellus degenerates before fertilization, while the other part persists until after fertilization (Xu *et al.*, 2016). Recently, it was reported that nucellar degeneration after pollination and before fertilization starts in the cells adjacent to the developing FG, and it is controlled by auxin (Wang *et al.*, 2021). Indeed, our IAA immunolocalization data suggest a dynamic and ordered influx and efflux of auxin in the nucellus after pollination and a disordered distribution of auxin in UO. This might cause the failure of the nucellar and FG normal development, with the consequent abortion of UO. Auxin efflux under control of PIN proteins is essential to achieve appropriate auxin maxima and for normal auxin signalling in a wide range of developmental processes, as demonstrated in *Arabidopsis* and maize (McSteen and Hake, 2001; Carraro *et al.*, 2006; Gallavotti *et al.*, 2008; Křeček *et al.*, 2009; Forestan *et al.*, 2012). Data analysis performed in this work has shown that four *PIN* genes, identified as *PIN3 Gb_03217*, *Gb_29191*, *Gb_02144*, and *PIN4 Gb_23207*, presented upregulation in the PO across the different time-points. Interestingly, only the expression of *PIN1 Gb_06199* showed a strong reduction as soon as the pollen was received, suggesting a possible post-pollination regulation mechanism. Moreover, ISH on *PIN1 Gb_06199* transcripts revealed different cyto-histological expression domains between PO and UO. Our results are in line with the current literature, which reports that auxin efflux carrier PIN1 transports auxin into the nucellus, while PIN3, PIN4 and PIN7 deliver auxin to degenerating nucellar cells and concomitantly control FG central vacuole expansion (Wang *et al.*, 2021). In *Arabidopsis*, the *pin1* mutant displays inhibited nucellar cells degeneration whereas *pin3/4/7* triple

mutant shows accelerated nucellar cell death but with reduced vacuolation, suggesting that auxin accumulation in the nucellus may promote PCD (Wang *et al.*, 2021). The evidence demonstrates the effect of auxin on PCD induced during plant development or by environmental factors (reviewed by Kacprzyk *et al.*, 2022).

Our results suggest that the hormonal regulatory pathways in *Ginkgo* ovules are similar to those found in angiosperms. Thus, we can hypothesise a conserved mechanism underlying this developmental process.

TFs as bridges linking pollen signalling and PCD control

TFs may act as bridges linking phytohormone signalling with PCD regulation (Li *et al.*, 2019).

Several homologs of the TFs associated with PCD have been identified as DEGs, including MYB and NAC TFs. Homologs of MYB (Plackett *et al.*, 2011) and bHLH (Ko *et al.*, 2014) have been known to promote tapetum PCD. MADS-box TFs were found to induce nucellar PCD during rice seed development (Yin *et al.*, 2012). Additionally, it was found that some NAC proteins function downstream of the ethylene signalling pathway to modulate the cascade of leaf senescence-associated PCD (Matallana-Ramirez *et al.*, 2012).

Our results also suggest the involvement of *Ginkgo* NAC TFs in the degeneration process of the nucellus and the FG in UO. The analysed *NAC* expression was mainly concentrated in the nucellus, which starts to degenerate approximately one week/10 days after the non-arrival of pollen. Among them, NAC *Gb_13930* seems to be mainly involved in FG degeneration because a strong signal was concentrated in that region. After all, the other studied NAC genes might be involved in the death process of the entire nucellus because of their more widespread expression in this tissue. This was supported by recent discovery in *Arabidopsis* ovules, in which the combined triple mutation of *NAC-LIKE ACTIVATED BY AP3/PI* (*NAP/ANAC029*), *SPEEDY HYPONASTIC GROWTH* (*SHYG*) and *ORESARA1* (*ORE1*) genes, which are the most expressed NAC at 4 days after emasculation, caused a delay in ovule senescence and an extension of fertility interval (Van Durme *et al.*, 2023). The expression of *Ginkgo NAC* in these tissues may indicate their involvement in the complete degradation and lignification of the nucellus and FG. It will be visible later after UO_8, which is considered in this study. This hypothesis is supported by the demonstrated requirement of NAM, CUC2, VND1-7, NST1 and NST2 in regulating the lignification process during xylem differentiation (Kubo *et al.*, 2005; Mitsuda *et al.*, 2005; Nakano *et al.*, 2015). Nevertheless, some of these transcripts were also observable in PO, especially in the contact region between the tapetum and the FG. This might be explainable because during the FG enlargement, at stage 9 of ovule

development, the tapetum surrounding the FG goes through PCD and degeneration (Douglas *et al.*, 2007; D'Apice *et al.*, 2021). The expression of senescence/PCD genes in the nucellus of PO is not surprising because at this stage, the nucellus rapidly degenerates due to the FG enlargement and the male gametophyte growth (D'Apice *et al.*, 2021). Regarding *MYB* genes, the most expressed gene was *Gb_39852*, which seems to be directly correlated with the degeneration of the nucellus and the adjacent portion of the integument in UO. Patzlaff *et al.* (2003) described that the R2R3-MYB gene of *Pinus taeda* (*PtMYB4*) was expressed only in cells which were destined to lignify suggesting that the selected MYB TFs seems to be associated with the lignification process.

Ovule abortion is the result of a different reprogramming of PCD, cell cycle and regulation of key genes affected by pollen

PCD is the genetic regulation of cell suicide, playing an essential role in multicellular organisms' development, homeostasis, and integrity (Ameisen, 2002).

In plants, three main types of PCD were reported: Apoptotic-like cell death (AL-PCD), senescence-associated death, and vacuole-mediated cell death, which resembles autophagy (Mondal *et al.*, 2021). In this work, most of the PCD-associated genes were categorised in the senescence pathway, which is a highly regulated process that requires the expression of many regulatory genes and involves the interaction of many signalling pathways (Buchanan-Wollaston, 2008).

Several genes involved in senescence were identified, and they were often referred to as SAGs or senescence-up-regulated genes. Some of the identified senescence-induced genes encode proteases, protease regulators, RNases, Gln synthetase, metallothioneins, glutathione *S*-transferase, catalase, ACC oxidase, lipases, glyoxylate cycle enzymes, endoxyloglucan transferase, pathogenesis-related proteins, ATP sulfurylase, Cyt P450, and polyubiquitin (Buchanan-Wollaston, 1997; Weaver *et al.*, 1997).

Here, the transcriptomic approach has shown the presence of two senescence key genes, *Gb_13610* and *Gb_10444*, strongly upregulated in UO, codifying for cysteine proteinase and KDEL- cysteine endopeptidase (KDEL CysEP) respectively, which are known to be involved in PCD (Beers *et al.*, 2000, 2004; Schaller, 2004). We focused on the *Gb_13610* cysteine proteinase, whose transcript was essentially revealed in the flap in both conditions. Unsurprisingly, *CYSP1* was found in tissues undergoing PCD, especially in cells that eventually collapse. Similar results were obtained in the unpollinated ovaries of *Pisum sativum* (Cercós *et al.*, 1999), in the outer integument developing into the seed coat of *Phalaenopsis* (Nadeau *et al.*, 1996), and in the megagametophyte cells after germination of *Picea glauca* seeds (He and Kermode, 2003). In *Brassica napus*, *BnCysp1* is associated with PCD of the inner integument of the ovule (Wan *et al.*, 2002).

On the other hand, because the whole FNMM process corresponds to continuous karyokinesis (Yao *et al.*, 2018; Zhang *et al.*, 2020), the abnormal FG development observed in UO suggested an anomaly in the cell cycle and its regulation, that alone or in concomitance with other mechanisms, leads to ovule abortion. Thus, *CDKB*, known for its function in regulating the cell cycle, was deeply investigated. The decreasing expression in UO detected for the *CDKB1* is in line with the general role of these proteins. Indeed, the DNA damage signals are transmitted via several proteins, suppressing the activity of cyclin-dependent kinase to arrest the cell cycle.

At last, in *Ginkgo* ovules, one senescence-associated event was the reduction in dimension after PD emission. Indeed, before abortion, UO already showed a reduced size, with respect to the pollinated ones, which exhibited exponential growth after PD emission. In addition, UO showed a large cavity between the nucellus and flap, suggesting the presence of several apoptotic cells in this portion. During PCD, the earliest sign of cellular disruption is DNA fragmentation (Kuthanova *et al.*, 2008). Indeed, through the TUNEL assay, we showed that DNA fragmentation started immediately at the UO_1 stage, with the signal accumulating at the base of the nucellus before the cavity became visible, confirming our hypothesis. In the last stages, DNA fragmentation affects other structures, including nucellar tissues and integuments, highlighting the massive presence of cells undergoing PCD.

Overall, the results confirmed our initial hypothesis that pollination inhibits the earliest PCD program in PO, leading to their proper development.

Given the complex network of molecular players described in this work, we have reported a scheme that shows how the pollination event is crucial for ovule development in *Ginkgo* and the cause of abortion in the unpollinated ovules (**Fig. 9**), with the aim of integrating all the results discussed here, and providing a useful reference for stimulating and establishing new studies of these processes in non-model plants.

ACKNOWLEDGEMENTS We are grateful to Maria Beatrice Bitonti for revising the manuscript. We thank Coretto Garden (Montalto Uffugo, CS, Italy) for providing us with the ovules of *Ginkgo biloba* L. isolated female plants.

AUTHOR CONTRIBUTIONS LB, BB, LC and FA planned and designed the study. AM, EG, ET, GD, SM, MDM, SN and NB performed the experiments and analysed the data. AM and ET analysed sequencing data. AM wrote the first draft. LB, BB, LC, AM, AC, SN, SM, MDM, ET, NB and FA provided critical editing of the manuscript.

CONFLICT OF INTEREST No conflict of interest was declared.

FUNDING This study was supported by MIUR PRIN (grant Prot. 20175R447S) and from the European Union's Horizon 2020 RISE program (Marie Skłodowska-Curie grant agreement no. 101007738).

DATA AVAILABILITY The datasets generated for this study can be found in the Sequence Read Archive (SRA) database at NCBI (SRA BioProject PRJNA700482) and within its Supplementary published online. Correspondence and requests for materials should be addressed to LB.

REFERENCES

Ambrose BA, Lerner DR, Ciceri P, Padilla CM, Yanofsky MF, Schmidt RJ. 2000. Molecular and genetic analyses of the *silky1* gene reveal conservation in floral organ specification between eudicots and monocots. Molecular Cell, **5**, 569–579.

Ameisen JC. 2002. On the origin, evolution, and nature of programmed cell death: a timeline of four billion years. Cell Death & Differentiation, **9**, 367-393.

Barro-Trastoy D, Dolores Gomez M, Tornero P, Perez-Amador MA. 2020. On the way to ovules: the hormonal regulation of ovule development. Critical Reviews in Plant Sciences, **39**, 431-456.

Beers EP, Jones AM, Dickerman AW. 2004. The S8 serine, C1A cysteine and A1 aspartic protease families in *Arabidopsis*. Phytochemistry **65**, 43–58.

Beers EP, Woffenden BJ, Zhao C. 2000. Plant proteolytic enzymes: possible roles during programmed cell death. Plant Molecular Biology **44**, 399–415.

Buchanan-Wollaston V. 1997. The molecular biology of leaf senescence. Journal of experimental botany, **48**, 181-199.

Buchanan-Wollaston V. 2008. Senescence processes in plants. Annual Plant Reviews, Volume 26. Annals of Botany **101**, 197.

Carraro N, Forestan C, Canova S, Traas J, Varotto S. 2006. *ZmPIN1a* and *ZmPIN1b* encode two novel putative candidates for polar auxin transport and plant architecture determination of maize. Plant Physiology **142**, 254–264.

Ceccato L, Masiero S, Sinha Roy D, Bencivenga S, Roig-Villanova I, Ditengou FA, Palme K, Simon R, Colombo L. 2013. Maternal control of PIN1 is required for female gametophyte development in *Arabidopsis*. PloS one, **8**, e66148.

Cercós M, Santamaría S, Carbonell J. 1999. Cloning and Characterization of *TPE4A*, a thiol-protease gene induced during ovary senescence and seed germination in pea. Plant Physiology **119**, 1341–1348.

Chen F, Zhang X, Liu X, Zhang L. 2017. Evolutionary analysis of MIKCc-Type MADS-Box genes in gymnosperms and angiosperms. Frontiers in Plant Science **8**, 895.

Chiappetta A, Fambrini M, Petrarulo M, *et al.* 2009. Ectopic expression of *LEAFY COTYLEDON1-LIKE* gene and localised auxin accumulation mark embryogenic competence in epiphyllous plants of *Helianthus annuus x H. tuberosus*. Annals of Botany **103**, 735–747.

Cucinotta M, Colombo L, Roig-Villanova I. 2014. Ovule development, a new model for lateral organ formation. Frontiers in Plant Science **5**, 117.

Cucinotta M, Cavalleri A, Chandler JW, Colombo L. 2021. Auxin and flower development: a blossoming field. Cold Spring Harbor Perspectives in Biology, **13**, a039974.

Cucinotta M, Di Marzo M, Guazzotti A, de Folter S, Kater MM, Colombo L. 2020. Gynoecium size and ovule number are interconnected traits that impact seed yield. Journal of Experimental Botany **71**, 2479–2489.

Daneva A, Gao Z, Van Durme M, Nowack MK. 2016. Functions and regulation of programmed cell death in plant development. Annual Review of Cell and Developmental Biology **32**, 441–468.

D'Apice G, Moschin S, Araniti F, Nigris S, Di Marzo M, Muto A, Banfi C, Bruno L, Colombo L, Baldan B. 2021. The role of pollination in controlling *Ginkgo biloba* ovule development. New Phytologist **232**, 2353–2368.

D'Apice G, Moschin S, Nigris S, Ciarle R, Muto A, Bruno L, Baldan B. 2022. Identification of key regulatory genes involved in the sporophyte and gametophyte development in *Ginkgo biloba* ovules revealed by in situ expression analyses. American Journal of Botany **109**, 887–898.

Dominguez F, Moreno J, Cejudo FJ. 2001. The nucellus degenerates by a process of programmed cell death during the early stages of wheat grain development. Planta, **213**, 352–360.

Dorcey E, Urbez C, Blázquez MA, Carbonell J, Perez-Amador MA. 2009. Fertilization-dependent auxin response in ovules triggers fruit development through the modulation of gibberellin metabolism in *Arabidopsis*. Plant Journal, **58**, 318–332.

Douglas AW, Stevenson DW, Little DP. 2007. Ovule Development in *Ginkgo biloba* L., with Emphasis on the Collar and Nucellus. International Journal of Plant Sciences **168**, 1207–1236.

Drews GN, Koltunow AMG. 2011. The Female Gametophyte. The Arabidopsis Book/American Society of Plant Biologists, **9**, e0155.

Figueiredo DD, Batista RA, Roszak PJ, Hennig L, Köhler C. 2016. Auxin production in the endosperm drives seed coat development in *Arabidopsis*. (R Amasino, Ed.). eLife **5**, e20542.

Figueiredo DD, Köhler C. 2018. Auxin: a molecular trigger of seed development. Genes & Development **32**, 479–490.

Forestan C, Farinati S, Varotto S. 2012. The maize PIN gene family of auxin transporters. Frontiers in Plant Science **3**, 16.

Friedman WE. 1987. Growth and development of the male gametophyte of *Ginkgo biloba* within the ovule (*in vivo*). American Journal of Botany **74**, 1797–1815.

Gallavotti A, Yang Y, Schmidt RJ, Jackson D. 2008. The relationship between auxin transport and maize branching. Plant Physiology **147**, 1913–1923.

Gao Z, Daneva A, Salanenka Y, *et al.* 2018. KIRA1 and ORESARA1 terminate flower receptivity by promoting cell death in the stigma of *Arabidopsis*. Nature plants **4**, 365–375.

Gao C, Yang R, Yuan D. 2017. Characteristics of developmental differences between fertile and aborted ovules in *Camellia oleifera*. Journal of the American Society for Horticultural Science **142**, 330–336.

Gong Z, Han R, Xu L, Hu H, Zhang M, Yang Q, Zeng M, Zhao Y, Zheng C. 2021. Combined transcriptome analysis reveals the ovule abortion regulatory mechanisms in the female sterile line of *Pinus tabuliformis* Carr. International Journal of Molecular Sciences **22**, 3138.

Guo Y, Zhang S, Li Y, Zhang X, Liu H, Liu S, Liu J, Wang G. 2023. A transcriptomic evaluation of the mechanism of programmed cell death of the replaceable bud in Chinese chestnut. Open life sciences **18**, 20220635.

He X, Kermode AR. 2003. Proteases associated with programmed cell death of megagametophyte cells after germination of white spruce (*Picea glauca*) seeds. Plant Molecular Biology **52**, 729–744.

Hollender CA, Kang C, Darwish O, Geretz A, Matthews BF, Slovin J, Alkharouf N, Liu Z. 2014. Floral transcriptomes in woodland strawberry uncover developing receptacle and anther gene networks. Plant Physiology **165**, 1062–1075.

Jin B, Wang D, Lu Y, Jiang XX, Zhang M, Zhang L, Wang L. 2012. Female short shoot and ovule development in *Ginkgo biloba* L. with emphasis on structures associated with wind pollination. International Scholarly Research Notices **2012**, e230685.

Kacprzyk J, Burke R, Schwarze J, McCabe PF. 2022. Plant programmed cell death meets auxin signalling. The FEBS journal **289**, 1731–1745.

Ko SS, Li MJ, Sun-Ben Ku M, *et al.* 2014. The bHLH142 transcription factor coordinates with TDR1 to modulate the expression of EAT1 and regulate pollen development in rice. The Plant Cell, **26**, 2486-2504.

Křeček P, Skůpa P, Libus J, Naramoto S, Tejos R, Friml J, Zažímalová E. 2009. The PIN-FORMED (PIN) protein family of auxin transporters. Genome Biology **10**, 249.

Kubo M, Udagawa M, Nishikubo N, Horiguchi G, Yamaguchi M, Ito J, Mimura T, Fukuda H, Demura T. 2005. Transcription switches for protoxylem and metaxylem vessel formation. Genes & Development **19**, 1855–1860.

Kuthanova A, Opatrny Z, Fischer L. 2008. Is internucleosomal DNA fragmentation an indicator of programmed death in plant cells? Journal of Experimental Botany, **59**, 2233–2240.

Langfelder P, Horvath S. 2008. WGCNA: an R package for weighted correlation network analysis. BMC Bioinformatics **9**, 559.

Larsson E, Vivian-Smith A, Offringa R, Sundberg E. 2017. Auxin homeostasis in *Arabidopsis* ovules is anther-dependent at maturation and changes dynamically upon fertilization. Frontiers in Plant Science **8**, 1735.

Lee CL. 1955. Fertilization in *Ginkgo biloba*. Botanical Gazette, **117**, 79-100.

Li D, Wu D, Li S, Guo N, Gao J, Sun X, Cai Y. 2019. Transcriptomic profiling identifies differentially expressed genes associated with programmed cell death of nucellar cells in *Ginkgo biloba* L. BMC plant biology, **19**, 1-17.

Li J, Wu Z, Cui L, *et al.* 2014. Transcriptome comparison of global distinctive features between pollination and parthenocarpic fruit set reveals transcriptional phytohormone cross-talk in cucumber (*Cucumis sativus* L.). Plant and Cell Physiology **55**, 1325–1342.

Li W, Li Q, Lyu M, *et al.* 2022. Lack of ethylene does not affect reproductive success and synergid cell death in *Arabidopsis*. Molecular Plant **15**, 354–362.

Lu Y, Zhang L, Cheng F, Zhao J, Cui J, Li W, Li W, Jin B. 2016. The morphology, ultrastructure, element distribution and motion behaviour in pollen of *Ginkgo biloba* L. Trees, **30**, 2189-2201.

Matallana-Ramírez LP. 2012. Unraveling the ORE1 regulon in *Arabidopsis thaliana*: molecular and functional characterization of up-and down-stream components. Elektronische Ressource. (Doctoral dissertation, Potsdam, Universität Potsdam, Diss., 2012).

McAtee P, Karim S, Schaffer R, David K. 2013. A dynamic interplay between phytohormones is required for fruit development, maturation, and ripening. Frontiers in Plant Science **4**, 79.

McSteen P, Hake S. 2001. barren inflorescence2 regulates axillary meristem development in the maize inflorescence. Development (Cambridge, England) **128**, 2881–2891.

Mitsuda N, Seki M, Shinozaki K, Ohme-Takagi M. 2005. The NAC transcription factors NST1 and NST2 of *Arabidopsis* regulate secondary wall thickenings and are required for anther dehiscence. The Plant Cell **17**, 2993–3006.

Mondal R, Antony S, Roy S, Chattopadhyay SK. 2021. Programmed cell death (PCD) in plant: molecular mechanism, regulation, and cellular dysfunction in response to development and stress. Regulation and dysfunction of apoptosis, **2**, 1-20.

Nadeau JA, Zhang XS, Li J, O'Neill SD. 1996. Ovule development: identification of stage-specific and tissue-specific cDNAs. The Plant Cell **8**, 213–239.

Nakano Y, Yamaguchi M, Endo H, Rejab NA, Ohtani M. 2015. NAC-MYB-based transcriptional regulation of secondary cell wall biosynthesis in land plants. Frontiers in Plant Science **6**, 288.

Ni X-L, Hou H, Xie Q, Zhang H, Yan P, Lv Y. 2022. Caspase 3-like protease is involved in ethylene-induced programmed cell death during aerenchyma formation in *Helianthus annuus* stem. Microscopy Research and Technique **85**, 3707–3715.

Patzlaff A, McInnis S, Courtenay A, *et al.* 2003. Characterisation of a pine MYB that regulates lignification. The Plant Journal: For Cell and Molecular Biology **36**, 743–754.

Plackett AR, Thomas SG, Wilson ZA, Hedden P. 2011. Gibberellin control of stamen development: a fertile field. Trends in plant science, **16**, 568-578.

Porceddu A, Stals H, Reichheld J-P, Segers G, Veylder LD, Barrôco R de P, Casteels P, Montagu MV, Inzé D, Mironov V. 2001. A plant-specific cyclin-dependent kinase is involved in the control of G2/M progression in plants. Journal of Biological Chemistry **276**, 36354–36360.

Prior N, Little SA, Boyes I, Griffith P, Husby C, Pirone-Davies C, Stevenson DW, Tomlinson PB, von Aderkas P. 2019. Complex reproductive secretions occur in all extant gymnosperm lineages: a proteomic survey of gymnosperm pollination drops. Plant Reproduction **32**, 153–166.

Rudall PJ. 2021. Evolution and patterning of the ovule in seed plants. Biological Reviews **96**, 943–960.

Schaller A. 2004. A cut above the rest: the regulatory function of plant proteases. Planta **220**, 183–197.

Schneider CA, Rasband WS, Eliceiri KW. 2012. NIH Image to ImageJ: 25 years of image analysis. Nature Methods **9**, 671–675.

Schubert R, Dobritzsch S, Gruber C, *et al.* 2019. Tomato MYB21 Acts in Ovules to Mediate Jasmonate-Regulated Fertility. The Plant Cell **31**, 1043–1062.

Shigyo M, Hasebe M, Ito M. 2006. Molecular evolution of the AP2 subfamily. Gene **366**, 256–265.

Sun H, Shi T, Song J, Xu Y, Gao Z, Song X, Ni Z, Cai B. 2016. Pistil abortion in Japanese apricot (*Prunus mume* Sieb. et Zucc.): isolation and functional analysis of PmCCoAOMT gene. Acta Physiologiae Plantarum **38**, 114.

Umeda M, Umeda-Hara C, Yamaguchi M, Hashimoto J, Uchimiya H. 1999. Differential expression of genes for cyclin-dependent protein kinases in rice plants. Plant Physiology **119**, 31–40.

van Doorn WG, Woltering EJ. 2008. Physiology and molecular biology of petal senescence. Journal of experimental botany, **59**, 453-480.

Van Durme M, Olvera-Carrillo Y, Pfeiffer ML, Doll NM, De Winter F, Lin Z, Nowack MK. 2023. Fertility loss in senescing *Arabidopsis* ovules is controlled by the maternal sporophyte via a NAC transcription factor triad. Proceedings of the National Academy of Sciences of the United States of America **120**, e2219868120.

Wan L, Xia Q, Qiu X, Selvaraj G. 2002. Early stages of seed development in *Brassica napus*: a seed coat-specific cysteine proteinase associated with programmed cell death of the inner integument. The Plant Journal: For Cell and Molecular Biology **30**, 1–10.

Wang J, Guo X, Xiao Q, Zhu J, Cheung AY, Yuan L, Vierling E, Xu S. 2021. Auxin efflux controls orderly nucellar degeneration and expansion of the female gametophyte in *Arabidopsis*. New Phytologist **230**, 2261–2274.

Weaver LM, Himelblau E, Amasino RM. 1997. Leaf senescence: gene expression and regulation. Genetic Engineering: Principles and Methods, **19**, 215-234.

Wetzstein HY, Yi W, Porter JA, Ravid N. 2013. Flower position and size impact ovule number per flower, fruitset, and fruit size in pomegranate. Journal of the American Society for Horticultural Science **138**, 159–166.

Xu W, Fiume E, Coen O, Pechoux C, Lepiniec L, Magnani E. 2016. Endosperm and nucellus develop antagonistically in *Arabidopsis* seeds. The Plant Cell **28**, 1343–1360.

Yadegari R, Drews GN. 2004. Female gametophyte development. The Plant Cell **16**, S133–S141.

Yamada T, Hirayama Y, Imaichi R, Kato M. 2008. *AINTEGUMENTA* homolog expression in *Gnetum* (gymnosperms) and implications for the evolution of ovulate axes in seed plants. Evolution & Development **10**, 280–287.

Yao Y, Han R, Gong Z, Zheng C, Zhao Y. 2018. RNA-Seq analysis reveals gene expression profiling of female fertile and sterile ovules of *Pinus tabulaeformis* Carr. during free nuclear mitosis of the female gametophyte. International journal of molecular sciences **19**, 2246.

Yin LL, Xue HW. 2012. The MADS29 transcription factor regulates the degradation of the nucellus and the nucellar projection during rice seed development. The Plant Cell, **24**, 1049-1065.

Zhang S, Dong R, Wang Y, Li X, Ji M, Wang X. 2021. NAC domain gene VvNAC26 interacts with VvMADS9 and influences seed and fruit development. Plant Physiology and Biochemistry **164**, 63–72.

Zhang M, Li W, Feng J, Gong Z, Yao Y, Zheng C. 2020. Integrative transcriptomics and proteomics analysis constructs a new molecular model for ovule abortion in the female-sterile line of *Pinus tabuliformis* Carr. Plant Science **294**, 110462.

Zhang M, Zheng C. 2016. Archegonium and fertilization in Coniferopsida. Trees **30**, 75–86.

Zumajo-Cardona C, Little DP, Stevenson D, Ambrose BA. 2021. Expression analyses in *Ginkgo biloba* provide new insights into the evolution and development of the seed. Scientific Reports **11**, 21995.

Figure legends

Fig. 1. Morphologic and microscopic observations of the *G. biloba* ovules over time (from April to May). **(A)** Growth kinetics of pollinated (PO) and unpollinated ovules (UO), considering the diameter of the ovule. Mean ± SD are represented as bars. The arrow, black for the PO and white for the UO, indicates the range of drop time emission. **(B-G)** Cytological observations during the three developmental stages analysed, 1 **(B, E)**, 6 **(C, F)**, and 8 **(D, G)** DAD in both PO **(B-D)** and UO **(E-G)** ovules. The histological sections were stained with blue toluidine. C, cavity; FG, female gametophyte; IN, integument; PC, pollen chamber; TA, tapetum. Scale bar = 500µm. Statistical significance of differences among values is indicated with different letters ($P<0.05$, ANOVA).

Fig. 2. Transcriptomic analysis changes considering libraries at all time points of pollinated and unpollinated libraries (UO/PO) at 1, 6, and 8DAD. **(A)** Differentially expressed genes (DEGs) considering the comparison between unpollinated/pollinated ovules and among three time points (UO_1/PO_1, UO_6/PO_6 and UO_8/PO_8, respectively). Gene expression level values were normalised by the DESEQ2 software (pvalue corrected < 0.05 and log2FC |1.5|). **(B)** Venn diagrams describing an overlapping of DEGs sets from pairwise comparisons of pollinated and unpollinated (UO_1 vs. PO_1, UO_6 vs. PO_6, UO_8 vs. PO_8). **(C)** Overlapping between the DEGs UO/PO list and "Pollination condition by WGCNA" (PCW) shows the main pathways impacted.

Fig. 3. Localization of *PIN1* (*Gb_06199*) transcripts by *in situ* hybridization with dig-labelled antisense probe (A-C, E-G). Longitudinal sections of pollinated (PO) **(A-C)** and unpollinated ovules (UO) **(E-G)** at stages 1 **(A-E)**, 6 **(B, F)** and 8 **(C, G)**. Signal is evidenced by purple staining **(A-F).** Longitudinal sections of PO and UO hybridised with *PIN1* sense probe **(D, H).** F, flap; FCL, flattened-cells layer; FG, female gametophyte; IN, integument; N, nucellus; PC, pollen chamber. **(A-E, H)** Scale bar = 500µm; **(F)** Scale bar = 200µm; **(G)** Scale bar = 100µm.

Fig. 4. Spatio-temporal distribution of free Indole-3-acetic acid (IAA) across ovule development stages. Immuno-reaction is evidenced as purple-violet staining. The signal was detected in longitudinal section in pollinated (PO) **(A, B, D, E, G, H)** and unpollinated ovules (UO) **(C, F, I)** at stages 1, **(A-C, E)** 6 **(D, F, H)** and 8 **(G, I)**. Magnification of FG **(D, E, H)** and pollen chamber **(B)** of pollinated ovules. **(J-K)** Longitudinal sections of ovules processed without primary antibody (negative control). C, cavity; FCL, flattened-cells layer; FG, female gametophyte; IN,

integument; M, micropyle; N, nucellus; PC, pollen chamber; TA, tapetum. **(A, C, D, F, I, J)** Scale bar = 500µm; **(B, G)** Scale bar = 200µm; **(E, H, K)** Scale bar = 100µm.

Fig. 5. Localization of selected *MYB* and *NAC* transcripts by *in situ* hybridization in longitudinal sections of pollinated (PO) and unpollinated (UO) ovules with dig-labelled antisense probes (A-N). *In situ* hybridizations of *G. biloba MYB Gb_15607* transcript in the stage PO_6 **(A)** and UO_6 **(B)**, *MYB Gb_02997* transcript in the stage PO_6 (**C**) and UO_6 (**D**) and *MYB Gb_39852* transcript in the stage PO_6 **(E)** and UO_6 ovules **(F)**. **(G-H)** Longitudinal sections of PO and UO hybridised with *MYB Gb_39852* sense probe. *In situ* hybridizations of *G. biloba NAC Gb_05670* transcript in the stage PO_6 (**I**) and UO_6 **(J)**, *NAC Gb_13930* transcript in the stage PO_6 (**K**) and UO_6 (**L**), *NAC Gb_35309* transcript in the stage PO_6 **(M)** and UO_6 **(N),** and *NAC Gb_18916* transcript in the stage PO_6 **(O)** and UO_6 **(P)**. Signal is evidenced by purple staining **(A-F; I-P)**. C, cavity; FG, female gametophyte; IN, integument; N, nucellus; PC, pollen chamber; TA, tapetum. **(A, C-P)** Scale bar = 500µm; **(B)** Scale bar = 200µm.

Fig. 6. Localization of *CYSP1* (*Gb_13610*) transcripts by *in situ* hybridization with dig-labelled antisense probe (A-C, E-G). Longitudinal sections of pollinated (PO) **(A-D)** and unpollinated ovules (UO) **(E-H)** at stages 1 **(A, E)**, 6 **(B, F)** and 8 **(C, G)**. Signal is evidenced by purple staining **(A-C, E-G).** Longitudinal sections of PO and UO hybridised with *CYSP1* sense probe **(D, H).** C, cavity; F, flap; FG, female gametophyte; IN, integument; PC, pollen chamber. **(B, C)** Scale bar = 700µm; **(A, D-H)** Scale bar = 500µm.

Fig. 7. Localization of *CDKB1* (*Gb_38629*) transcripts by *in situ* hybridization with dig-labelled antisense probe (A-F). Longitudinal sections of pollinated (PO) **(A-C)** and unpollinated ovules (UO) **(D-F)** at stages 1 **(A, D)**, 6 **(B, E)** and 8 **(C, F)**. Signal is evidenced by purple staining **(A-F).** Longitudinal sections of PO and UO hybridised with *CDKB1* sense probe **(G, H)**. C, cavity; F, flap; FG, female gametophyte; IN, integument; M, micropyle; N, nucellus; PC, pollen chamber. **(A-H)** Scale bar = 500µm.

Fig. 8. DNA degradation in nuclei from pollinated and unpollinated ovules. Nuclear DNA fragmentation was visualised *in situ* using TUNEL staining on longitudinal paraffin sections in pollinated (PO) **(A-C)** and unpollinated (UO) **(D-F)** ovules at stages 1 **(A, D),** 6 **(B, E)** and 8 **(C, F).** Green colour indicates nuclear DNA fragmentation. Nuclei were counterstained with DAPI (blue colour). C, cavity; F, flap; FCL, flattened-cells layer; FG, female gametophyte; IN, integument; M, mycropile; PC, pollen chamber. **(A-D)** Scale bar = 500 µm; **(E-F)** Scale bar = 200µm.

Fig. 9. Simplified scheme representing how the pollination event is crucial for ovule development in *G. biloba.* Pollen captured by the pollination drop blocks the cyto-histological disorganisation of the ovule and allows ovule development progression. On the contrary, ovules from female *G. biloba* plants that were geographically isolated and did not receive pollen gradually aborted all their ovules after the emission of the pollination drop due to cyto-histological disorganisation. In pollinated ovules (PO), ordered auxin distribution and upregulation of key genes involved in cell cycle and mitosis, DNA replication and damage repair were observed. In addition, genes associated with PCD and senescence were downregulated. Overall, this genetic network is likely to be involved in gametophyte expansion and nucellar degeneration. The opposite trend in gene expression was observed in unpollinated ovules (UO), which showed gametophyte degeneration, cytohistological alterations and finally abortion.

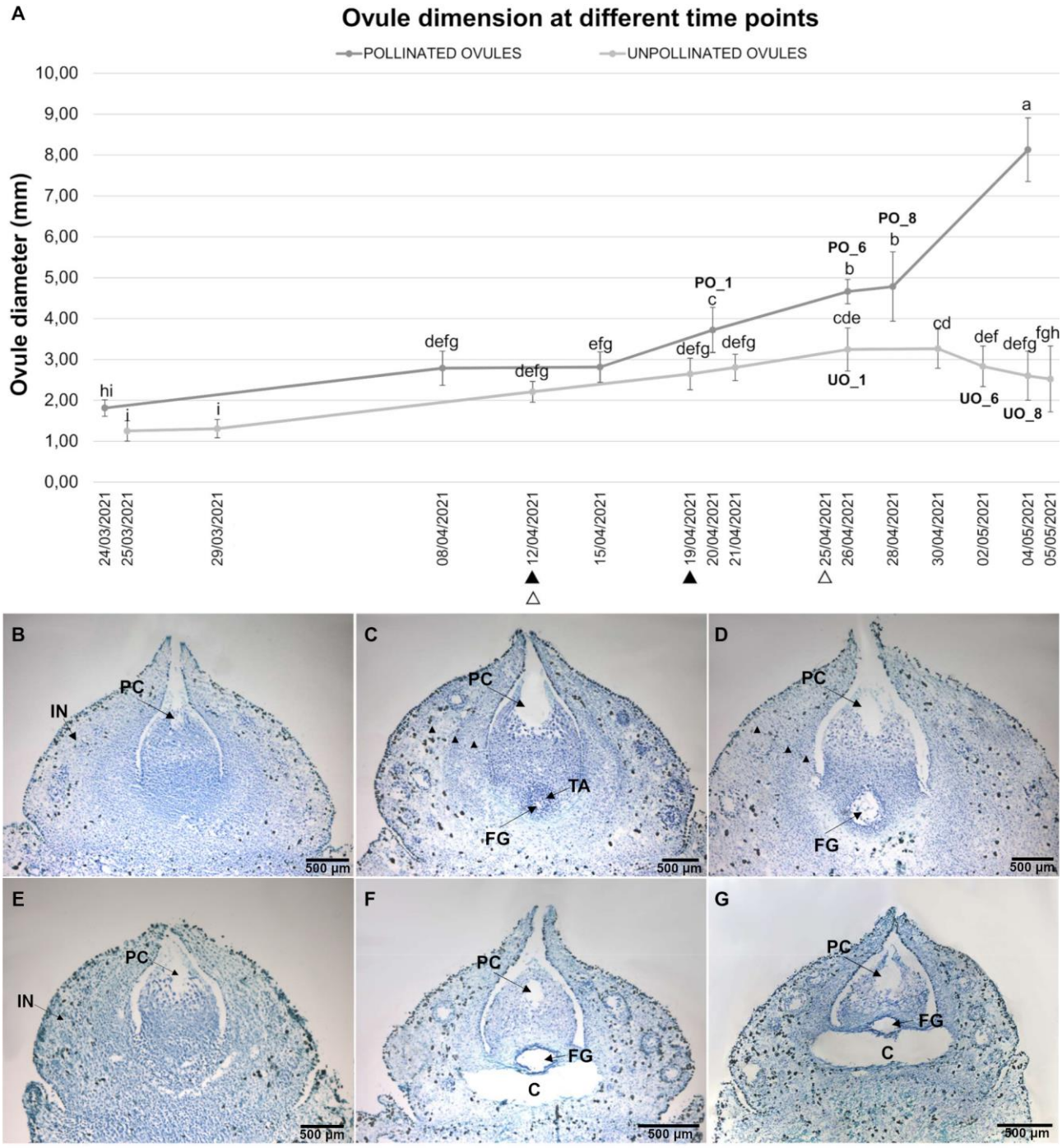

Fig. 1. Morphologic and microscopic observations of the *G. biloba* ovules over time (from April to May). (A) Growth kinetics of pollinated (PO) and unpollinated ovules (UO), considering the diameter of the ovule. Mean ± SD are represented as bars. The arrow, black for the PO and white for the UO, indicates the range of drop time emission. **(B-G)** Cytological observations during the three developmental stages analysed, 1 **(B, E)**, 6 **(C, F)**, and 8 **(D, G)** DAD in both PO **(B-D)** and UO **(E-G)** ovules. The histological sections were stained with blue toluidine. C, cavity; FG, female gametophyte; IN, integument; PC, pollen chamber; TA, tapetum. Scale bar = 500µm. Statistical significance of differences among values is indicated with different letters ($P<0.05$, ANOVA).

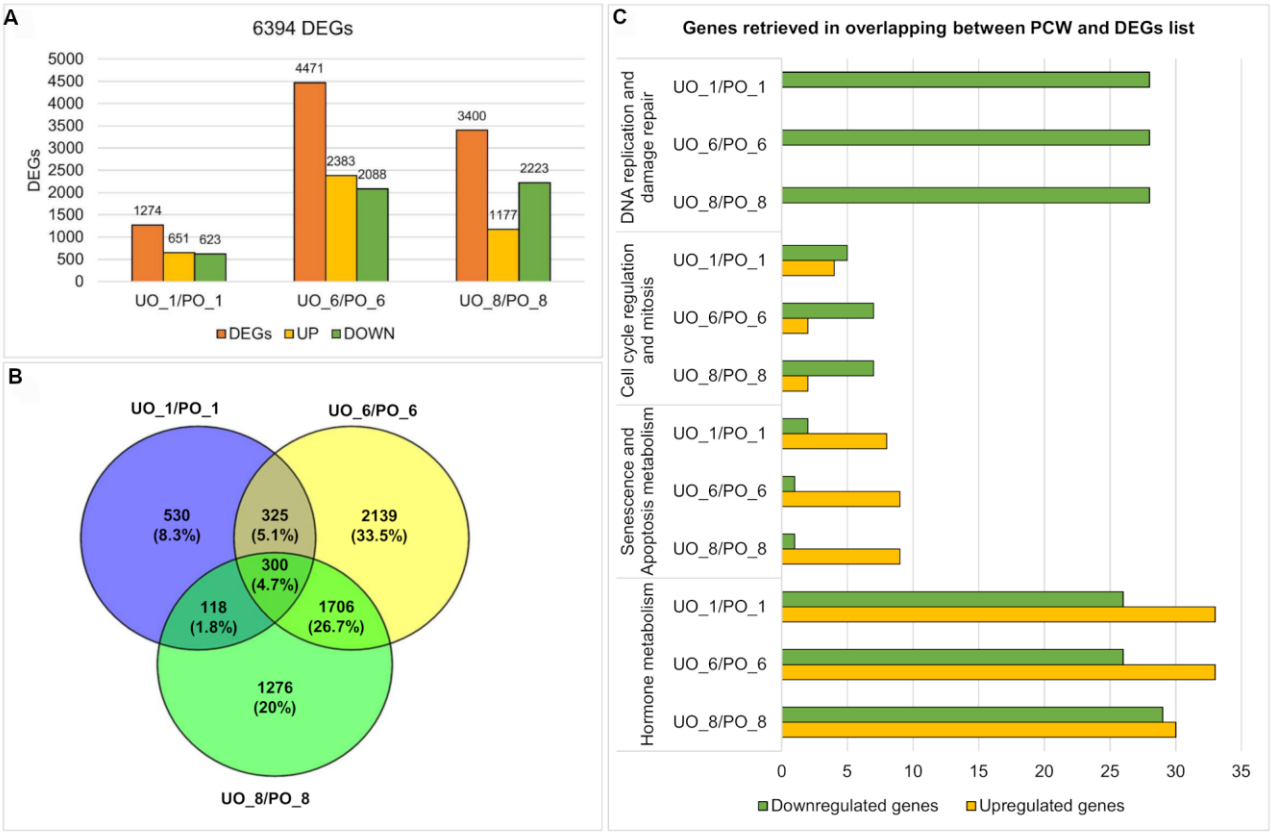

Fig. 2. Transcriptomic analysis changes considering libraries at all time points of pollinated and unpollinated libraries (UO/PO) at 1, 6, and 8DAD. (A) Differentially expressed genes (DEGs) considering the comparison between unpollinated/pollinated ovules and among three time points (UO_1/-PO_1, UO_6/PO_6 and UO_8/PO_8, respectively). Gene expression level values were normalised by the DESEQ2 software (pvalue corrected < 0.05 and log2FC |1.5|). **(B)** Venn diagrams describing an overlapping of DEGs sets from pairwise comparisons of pollinated and unpollinated (UO_1 vs. PO_1, UO_6 vs. PO_6, UO_8 vs. PO_8). **(C)** Overlapping between the DEGs UO/PO list and "Pollination condition by WGCNA" (PCW) shows the main pathways impacted.

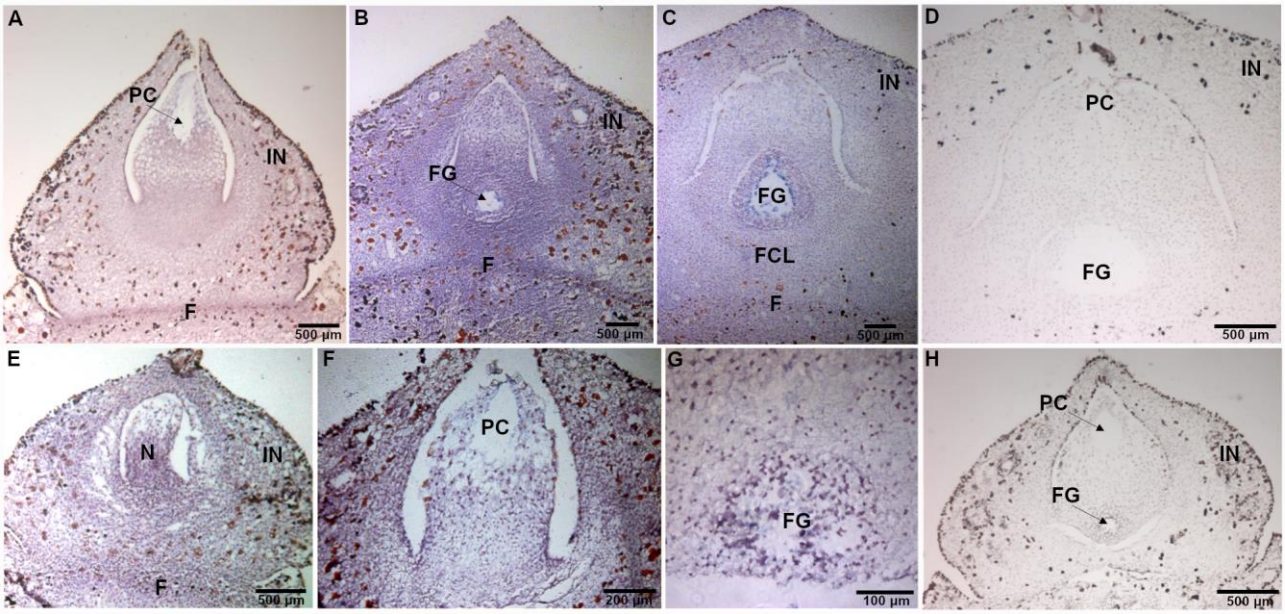

Fig. 3. Localization of *PIN1* (*Gb_06199*) transcripts by *in situ* hybridization with dig-labelled antisense probe (A-C, E-G). Longitudinal sections of pollinated (PO) **(A-C)** and unpollinated ovules (UO) **(E-G)** at stages 1 **(A-E)**, 6 **(B, F)** and 8 **(C, G)**. Signal is evidenced by purple staining **(A-F)**. Longitudinal sections of PO and UO hybridised with *PIN1* sense probe **(D, H)**. F, flap; FCL, flattened-cells layer; FG, female gametophyte; IN, integument; N, nucellus; PC, pollen chamber. **(A-E, H)** Scale bar = 500µm; **(F)** Scale bar = 200µm; **(G)** Scale bar = 100µm.

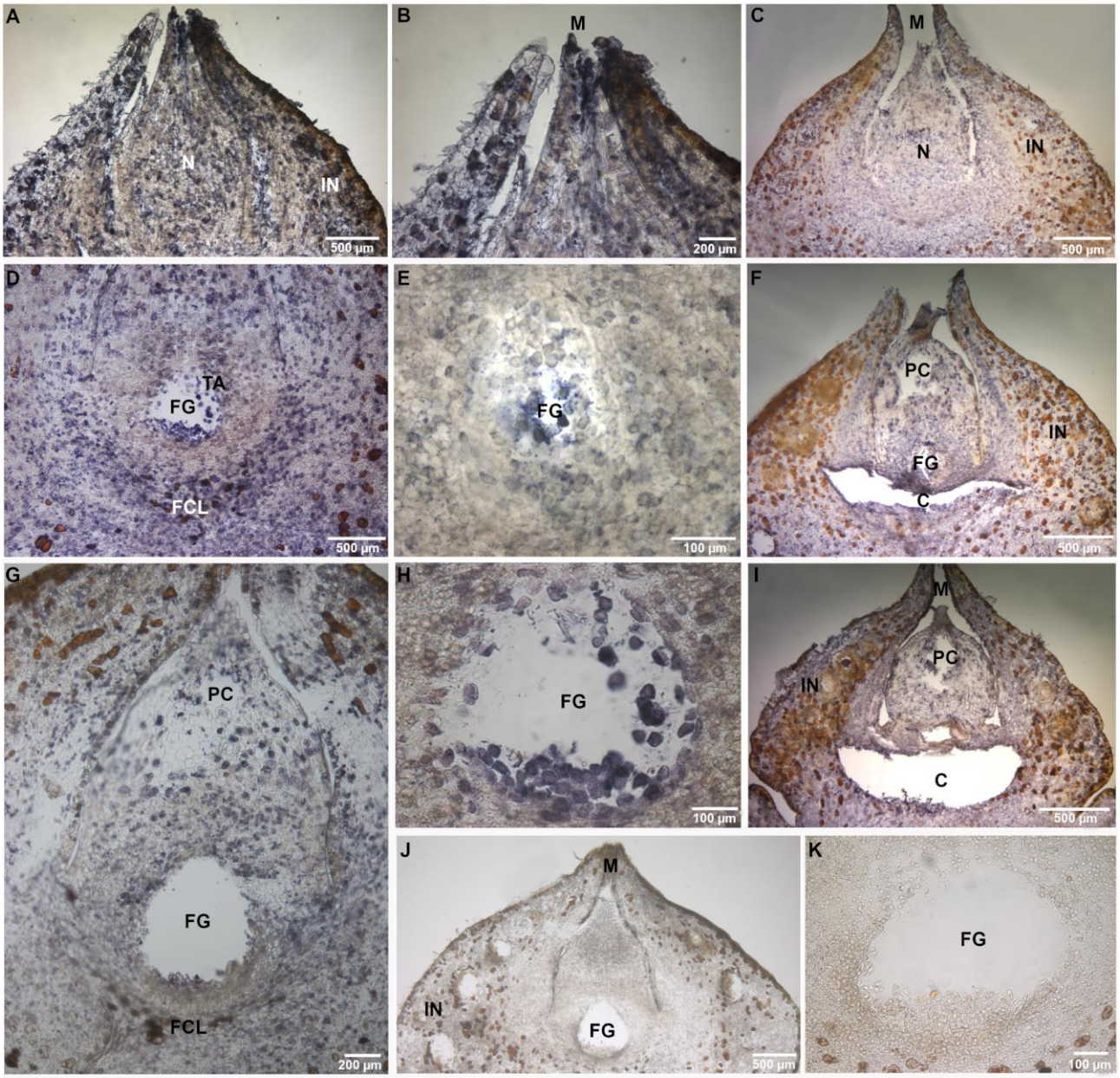

Fig. 4. Spatio-temporal distribution of free Indole-3-acetic acid (IAA) across ovule development stages. Immuno-reaction is evidenced as purple-violet staining. The signal was detected in longitudinal section in pollinated (PO) **(A, B, D, E, G, H)** and unpollinated ovules (UO) **(C, F, I)** at stages 1, **(A-C, E)** 6 **(D, F, H)** and 8 **(G, I)**. Magnification of FG **(D, E, H)** and pollen chamber **(B)** of pollinated ovules. **(J-K)** Longitudinal sections of ovules processed without primary antibody (negative control). C, cavity; FCL, flattened-cells layer; FG, female gametophyte; IN, integument; M, micropyle; N, nucellus; PC, pollen chamber; TA, tapetum. **(A, C, D, F, I, J)** Scale bar = 500µm; **(B, G)** Scale bar = 200µm; **(E, H, K)** Scale bar = 100µm.

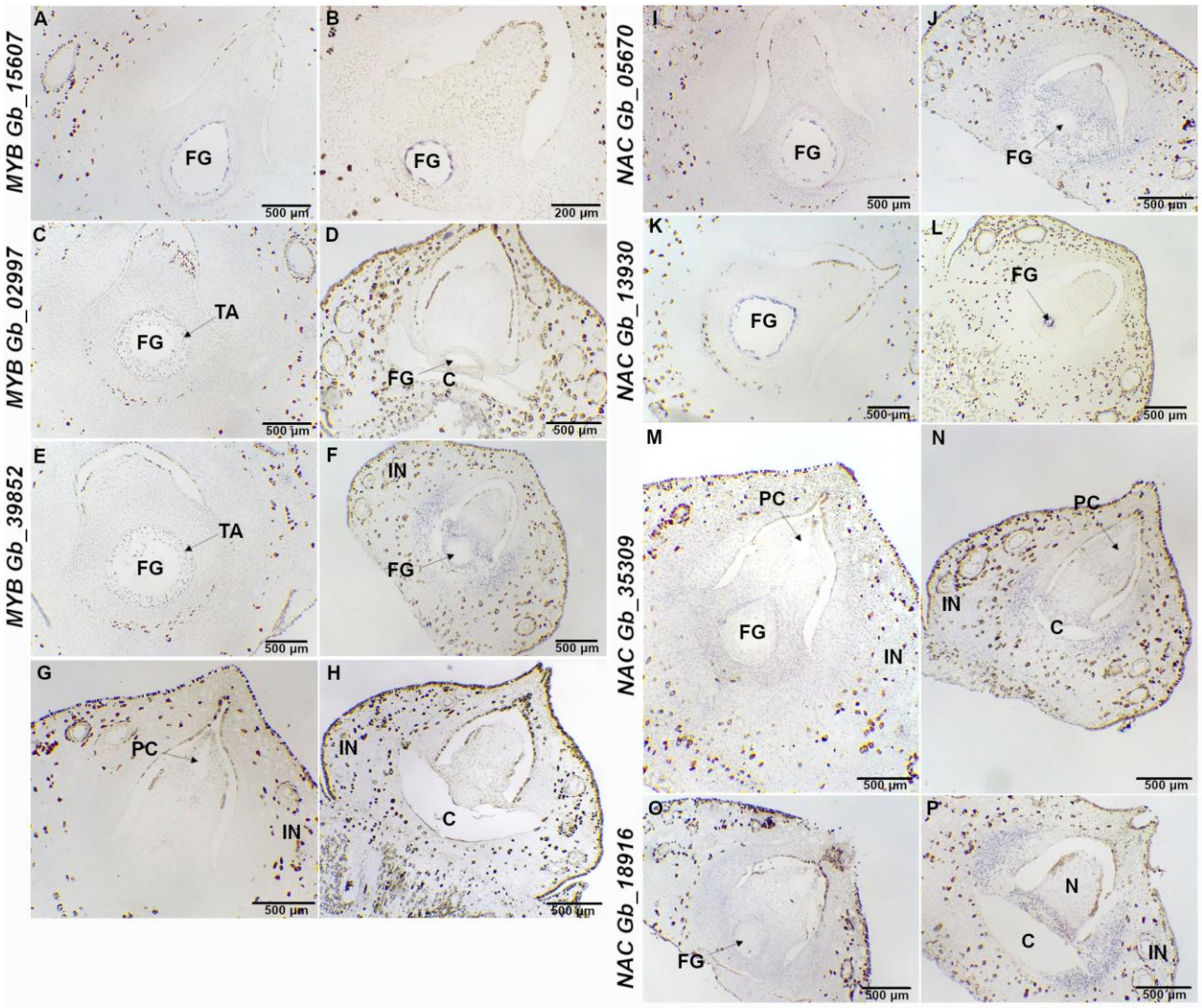

Fig. 5. Localization of selected *MYB* and *NAC* transcripts by *in situ* hybridization in longitudinal sections of pollinated (PO) and unpollinated (UO) ovules with dig-labelled antisense probes (A-N). *In situ* hybridizations of *G. biloba MYB Gb_15607* transcript in the stage PO_6 **(A)** and UO_6 **(B)**, *MYB Gb_02997* transcript in the stage PO_6 **(C)** and UO_6 **(D)** and *MYB Gb_39852* transcript in the stage PO_6 **(E)** and UO_6 ovules **(F)**. **(G-H)** Longitudinal sections of PO and UO hybridised with *MYB Gb_39852* sense probe. *In situ* hybridizations of *G. biloba NAC Gb_05670* transcript in the stage PO_6 **(I)** and UO_6 **(J)**, *NAC Gb_13930* transcript in the stage PO_6 **(K)** and UO_6 **(L)**, *NAC Gb_35309* transcript in the stage PO_6 **(M)** and UO_6 **(N)**, and *NAC Gb_18916* transcript in the stage PO_6 **(O)** and UO_6 **(P)**. Signal is evidenced by purple staining **(A-F; I-P)**. C, cavity; FG, female gametophyte; IN, integument; N, nucellus; PC, pollen chamber; TA, tapetum. **(A, C-P)** Scale bar = 500µm; **(B)** Scale bar = 200µm.

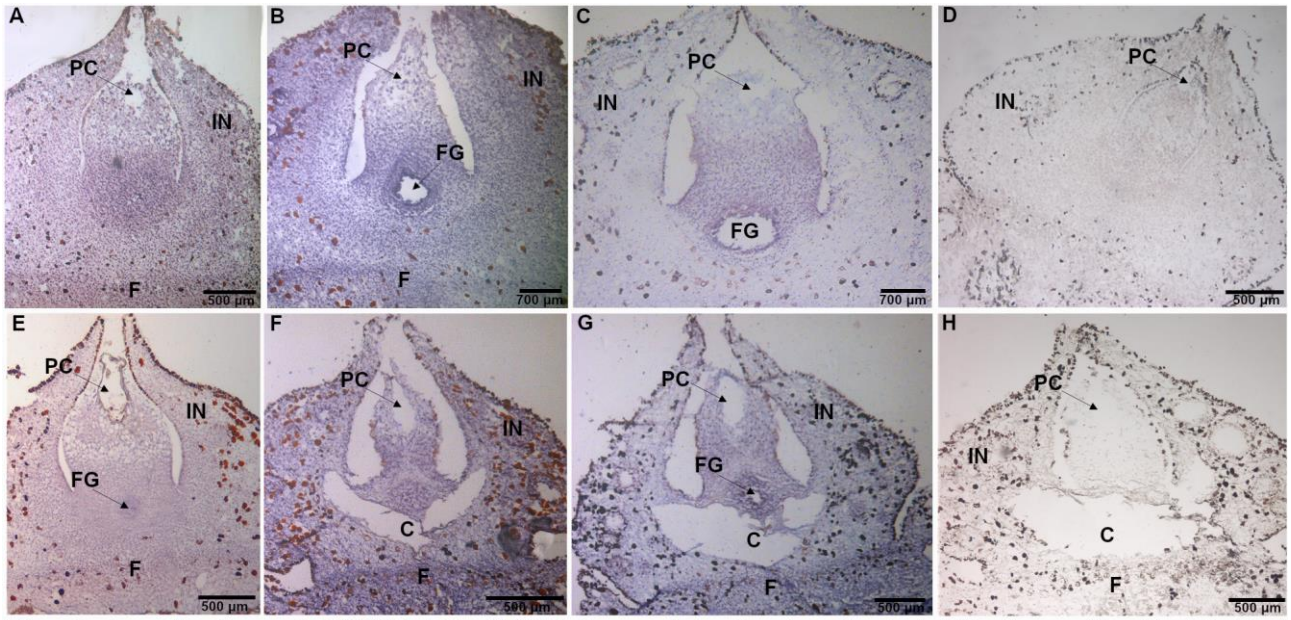

Fig. 6. Localization of *CYSP1* (*Gb_13610*) transcripts by *in situ* hybridization with dig-labelled antisense probe (A-C, E-G). Longitudinal sections of pollinated (PO) **(A-D)** and unpollinated ovules (UO) **(E-H)** at stages 1 **(A, E)**, 6 **(B, F)** and 8 **(C, G)**. Signal is evidenced by purple staining **(A-C, E-G)**. Longitudinal sections of PO and UO hybridised with *CYSP1* sense probe **(D, H)**. C, cavity; F, flap; FG, female gametophyte; IN, integument; PC, pollen chamber. **(B, C)** Scale bar = 700µm; **(A, D-H)** Scale bar = 500µm.

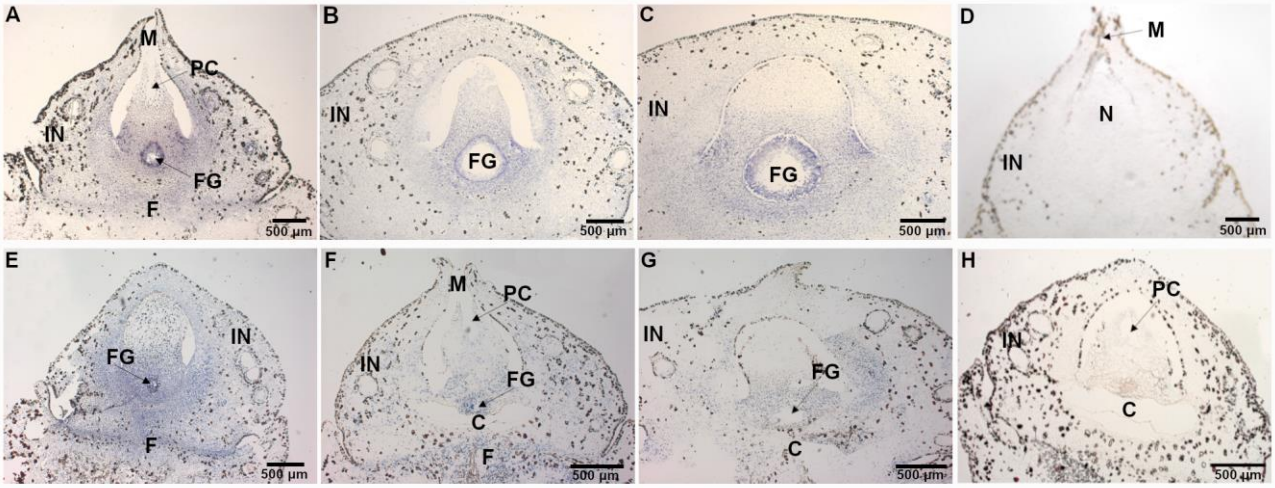

Fig. 7. Localization of *CDKB1* (*Gb_38629*) transcripts by *in situ* hybridization with dig-labelled antisense probe (A-F). Longitudinal sections of pollinated (PO) **(A-C)** and unpollinated ovules (UO) **(D-F)** at stages 1 **(A, D)**, 6 **(B, E)** and 8 **(C, F)**. Signal is evidenced by purple staining **(A-F)**. Longitudinal sections of PO and UO hybridised with *CDKB1* sense probe **(G, H)**. C, cavity; F, flap; FG, female gametophyte; IN, integument; M, micropyle; N, nucellus; PC, pollen chamber. **(A-H)** Scale bar = 500µm.

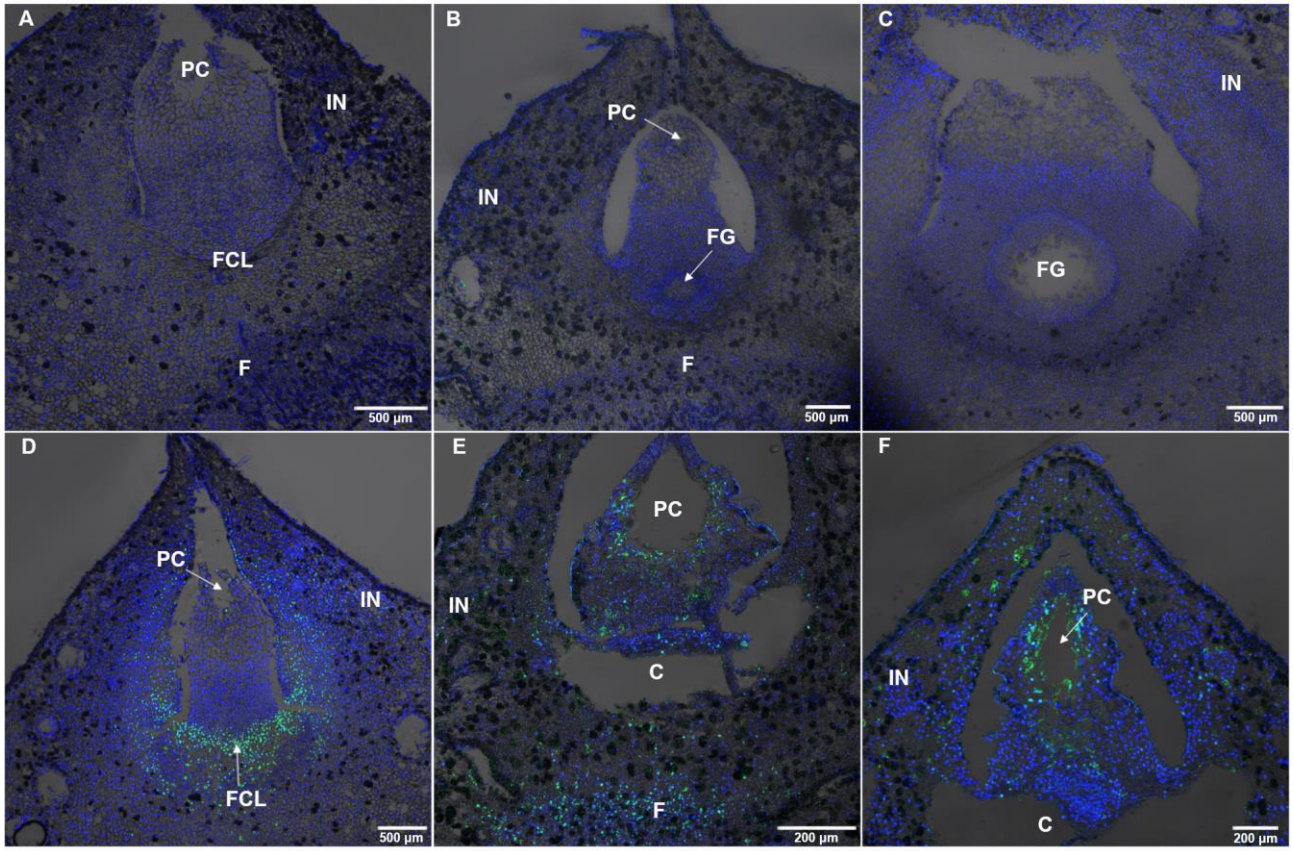

Fig. 8. DNA degradation in nuclei from pollinated and unpollinated ovules. Nuclear DNA fragmentation was visualised *in situ* using TUNEL staining on longitudinal paraffin sections in pollinated (PO) **(A-C)** and unpollinated (UO) **(D-F)** ovules at stages 1 **(A, D)**, 6 **(B, E)** and 8 **(C, F)**. Green colour indicates nuclear DNA fragmentation. Nuclei were counterstained with DAPI (blue colour). C, cavity; F, flap; FCL, flattened-cells layer; FG, female gametophyte; IN, integument; M, mycropile; PC, pollen chamber. **(A-D)** Scale bar = 500 µm; **(E-F)** Scale bar = 200µm.

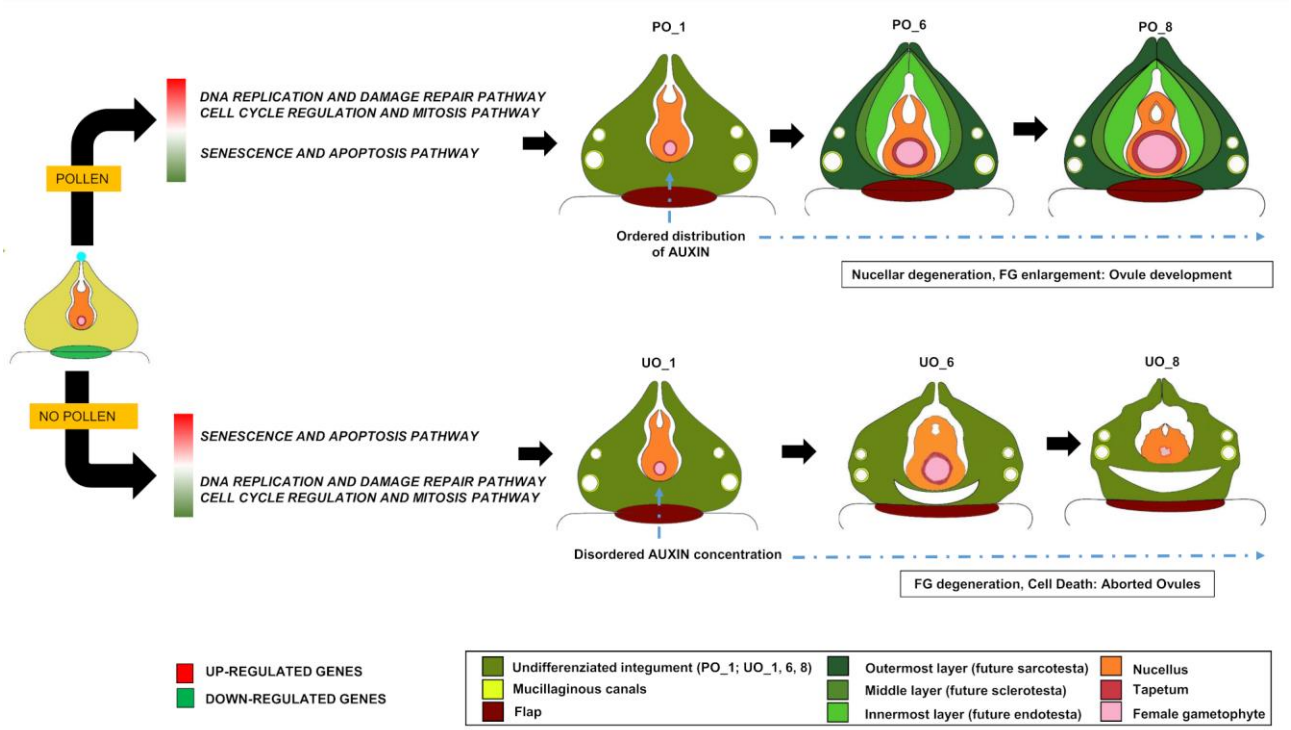

Fig. 9. Simplified scheme representing how the pollination event is crucial for ovule development in *G. biloba*. Pollen captured by the pollination drop blocks the cyto-histological disorganisation of the ovule and allows ovule development progression. On the contrary, ovules from female *G. biloba* plants that were geographically isolated and did not receive pollen gradually aborted all their ovules after the emission of the pollination drop due to cyto-histological disorganisation. In pollinated ovules (PO), ordered auxin distribution and upregulation of key genes involved in cell cycle and mitosis, DNA replication and damage repair were observed. In addition, genes associated with PCD and senescence were downregulated. Overall, this genetic network is likely to be involved in gametophyte expansion and nucellar degeneration. The opposite trend in gene expression was observed in unpollinated ovules (UO), which showed gametophyte degeneration, cytohistological alterations and finally abortion.